Integrating Sphere Homogeneity and the Relative Brightness of each DISR Instrument's Calibration Field

Bashar Rizk

16 August 2000, rev. 17 May 2002

Introduction

This report describes how the results of the map of the DISR calibration integrating sphere's brightness homogeneity are employed to derive individual window-centered relative brightness maps within each DISR instrument's field of view interior to the sphere. These maps can then be integrated or sampled depending on how each instrument behaves. Readers desiring some background on the measurements and issues behind the inhomogeneity of the calibration sphere's radiance field should read Appendix A. The discussion below assumes a basic familiarity with the results of this appendix. The overall goal of this effort, at least as far as the absolute calibration of the DISR instruments is concerned, is presented in Appendix B, as well as in the tables of Appendix C.

Integrating Sphere Relative Brightness Map and Sphere-Centered Coordinate System

As reviewed in Appendix A, the integrating sphere relative brightness map was derived from a set of measurements acquired in 1996 by a Si detector mounted on a turret and ball assembly that was part of a structure with the same dimensions, color and texture as the DISR Sensor Head. When inserted into the DISR calibration sphere, this dummy Sensor Head is assumed to shape the radiance field inside to be the same as during actual absolute responsivity calibrations. Once inside, the brightness everywhere within the sphere is measured (except in the immediate area of the dummy sensor head) and the results expressed in an array on a 1^{o}-grid in zenith and azimuth angle covering the whole sphere.

Figure 1

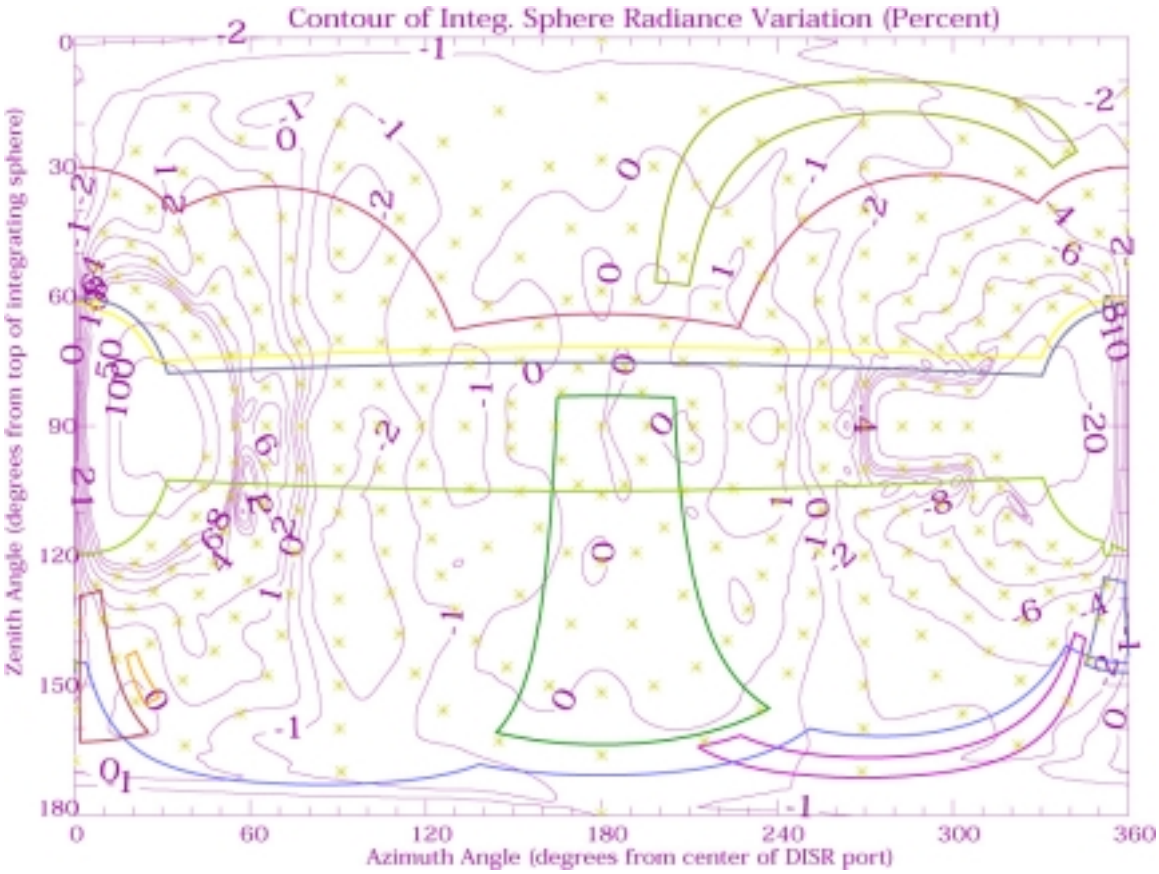

Figure 1 displays the relative intensity of light inside the sphere when illuminated by the high-intensity lamp through Port 5, the standard method of injecting photons during the DISR sphere-related calibrations, which included absolute responsivity, relative spectral responsivity, temperature sensitivity and cross-talk. The results are expressed in % deviation from the location at the front of the sphere (θ=90°, ϕ=180°), the spot directly opposite the DISR Sensor Head. For example, a 1% positive deviation represents a region that is 1% brighter than the exact front of the sphere. Also displayed are the 316 points where measurements occur, denoted by asterisks, and the outlines of the fields of view of the various DISR instruments. Refer to Table 1 in Appendix A for the specifications of the pointing and fields of view of the various DISR instruments.

Figure 2

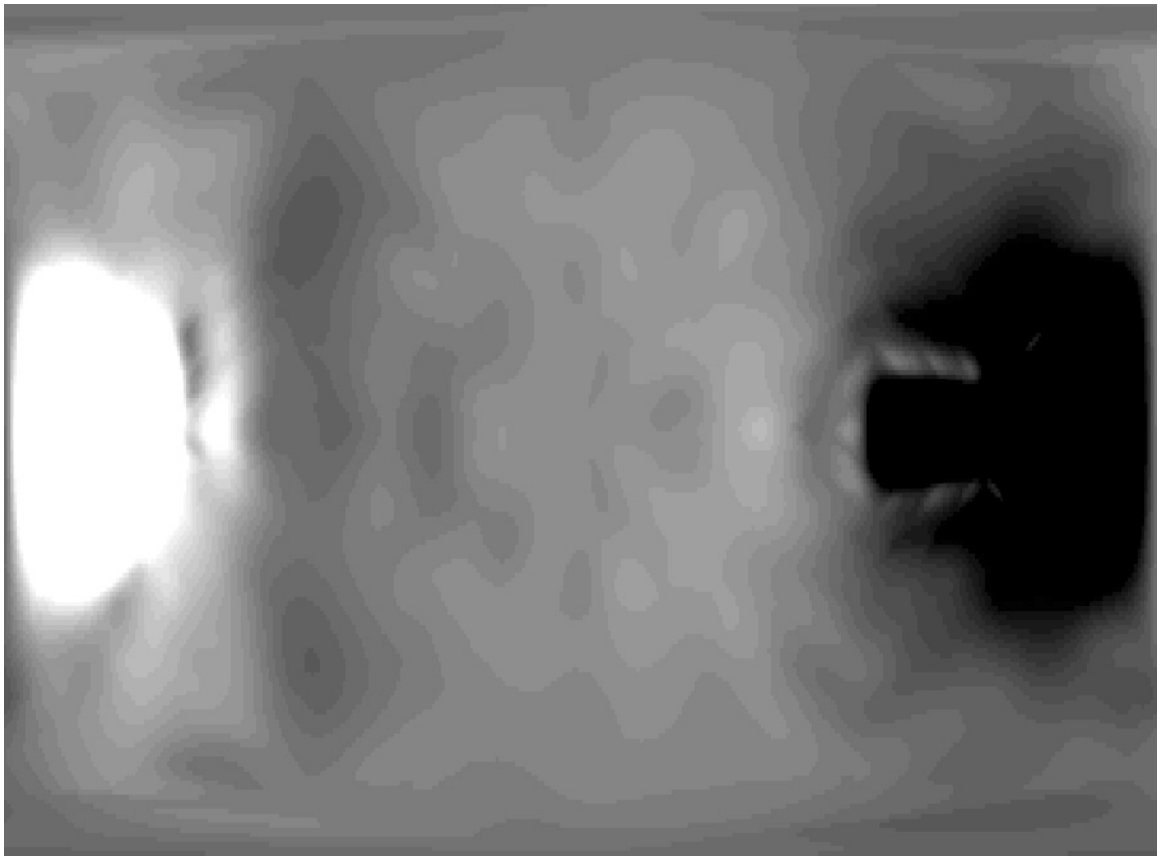

Figure 2 presents a grayscale image of the information in Figure 1. The data is presented on a spherical grid spanned by two angles: the zenith angle and azimuth angle, based on a spherical coordinate system with its origin at the center of the sphere. The zenith angle is defined as 0^o at the top of the sphere and 180^o at the bottom. The equator is at zenith 90^o. The azimuth angle is defined as 0^o at the DISR Sensor Head location and increases counterclockwise around the sphere to 360^o back at the Sensor Head. If one stands at the position of the Sensor Head and looks into the sphere through the main port, then azimuth angle increases towards one's right-hand side. As a right-handed Cartesian coordinate system, the x-axis points toward the DISR Sensor Head, the y-axis points to azimuth angle 90^o, zenith angle 90^o and the z-axis points to the top of the sphere at zenith angle 0^o. It is referred to as the **sphere-centered** coordinate system.

The current path to the relative brightness data is /cassini/users/bashar/calibration/reduction/shomo/bb_red8_ratio.dat, an ASCII file.

DISR Windows Centers and DISR Coordinate System

The center of each DISR instrument window is located within the **DISR SH-centered** coordinate system in mm. These centers are presented in Table 1. The origin of the sphere (the center) in this system is located at (53.25, 74.4, 398.2) mm.

Table 1

Instrument	X (mm)	Y (mm)	Z (mm)
DLVS	18.566	25.976	209.732
ULVS/ULV	101.617	45.989	173.388
HRI	8.067	56.172	187.101
MRI	17.629	49.183	208.288
SLI	46.382	52.752	224.475
SA1	93.378	42.949	199.412
SA2	89.127	42.949	202.979
SA3	84.913	42.949	206.515
SA4	80.662	42.949	210.082
DLVS	3.956	45.418	173.388
ULIS	116.467	103.418	173.388
DLIS	18.332	125.482	207.980
SS	87.336	81.481	204.155
SSL	17.915	93.481	195.645
Sphere	53.25	74.4	398.2

The DISR SH coordinate system is a right-handed Cartesian coordinate system, centered at the center of DISR's Sensor Head's left mounting foot (left if one is standing at the DISR Sensor Head's position and looking in the direction in which its business end points), in which the x-axis points straight up, the z-axis points in the direction in which the DISR SH looks and the y-axis points toward the right, in toward the main body of the instrument (in the direction of $\hat{z} \times \hat{x}$).

FOV Brightness Variations and Window-Centered Coordinate System

The brightness variations within the FOV of each DISR instrument are expressed on a spherical grid of zenith angle and azimuth angle centered at the window, called the **window-centered** system. In such a system, the zenith angle is 0^o straight up, 90^o at the equator and 180^o at nadir, or straight down. The azimuth angle starts at 0^o on the right-hand-side of an observer who sits at the position of the instrument in question and looks out into the direction it sees, and increases to the left (counterclockwise) till it reaches 180^o at the left-hand-side of the instrument's FOV. Zenith angle 90^o, azimuth angle 90^o is the direction straight ahead in this coordinate system.

The x-axis of this system points along the direction zenith 90^o and azimuth 0^o, or the right-hand side of the FOV. The y-axis points straight ahead. The z-axis points straight up.

Relationships between the Three Coordinate Systems

Figure 3 displays the three coordinate systems.

Figure 3

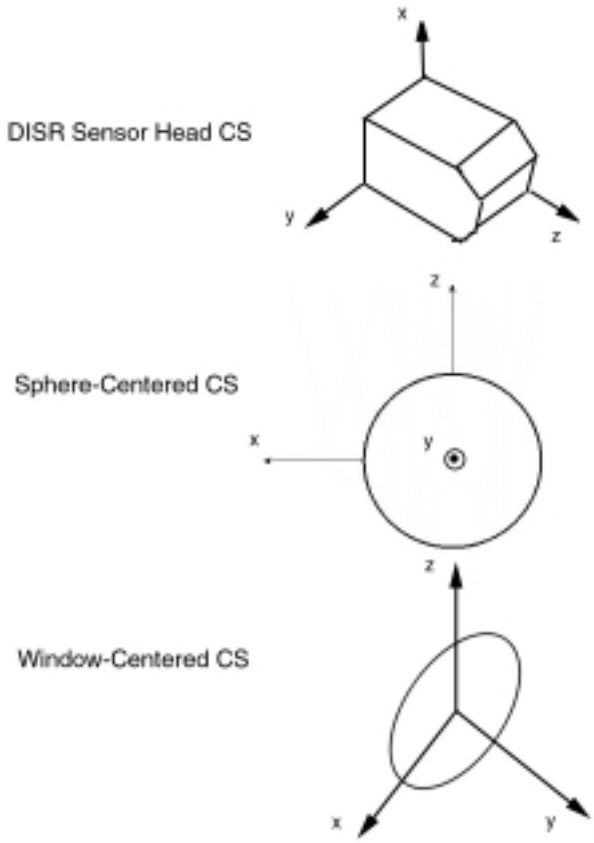

In the sphere- and window-centered cases the Cartesian systems are related to the resulting spherical coordinate systems in the conventional manner. Azimuth angle is measured in the x-y plane, beginning with 0° at the x-axis and increasing counterclockwise to 90° at the y-axis. Zenith angle is 0° at the z-axis and increases downward to 180o at –z. The equations relating Cartesian to spherical are therefore

$$x = r\sin\theta\cos\phi$$
$$y = r\sin\theta\sin\phi$$
$$z = r\cos\theta$$

In the DISR Sensor Head case, y takes the place of -x, z substitutes for y and x for z. Azimuth 0° is usually taken to lie along the z-axis, which corresponds to the optical axis of most of the DISR instruments. The resulting conversions are given as

$$x = r\cos\theta$$
$$y = -r\sin\theta\sin\phi$$
$$z = r\sin\theta\cos\phi$$

The Cartesian equations relating the three systems to each other follow:

1) DISR SH to sphere-centered

$$x = -z$$
$$y = y$$
$$z = x$$

2) DISR SH to window-centered

$$x = y$$
$$y = z$$
$$z = x$$

3) Sphere-centered to window-centered

$$x = y$$
$$y = -x$$
$$z = z$$

Note that in most cases, the fact that the DISR Sensor Head sits at the main port of the integrating sphere means that the window-centered, sphere-centered and DISR-centered systems are aligned with each other, though turned 90° one way or the other. In cases where the FOV of an instrument (e.g., the monochromator) that is mounted at one of the auxiliary ports is being considered, then the amount of the misalignment is not 90°, but something else (in the case of the monochromator it is 60°). This misalignment angle must then be included explicitly in the equations relating the window-centered system to the other two.

Converting the Relative Brightness Data from the Sphere-Centered to the Window-Centered System

Measuring the calibration sphere's internal brightness as a function of location inside the sphere provides a means for correcting the absolute responsivity calibrations of the various DISR instruments for the sphere's internal radiance inhomogeneity. To properly use the relative brightness data, which is derived on a sphere-centered grid, the data must be converted to a window-centered grid for each DISR instrument. Both systems are defined above.

Figure 4

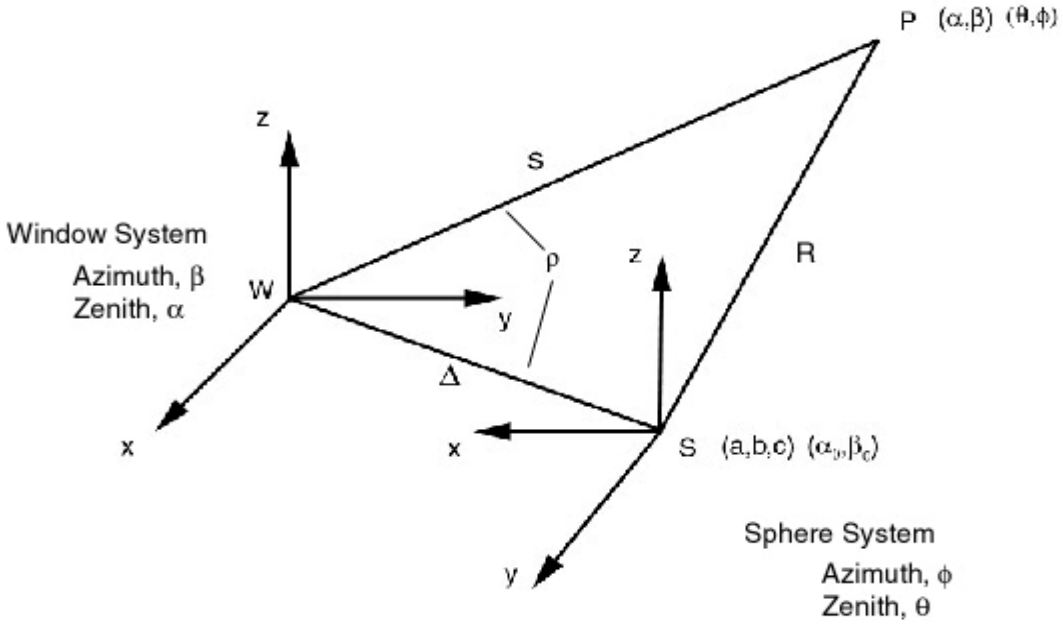

The procedure for conversion is complicated by the fact that because the grid desired is window-centered and not sphere-centered, the distance to the point where the brightness is needed is not known beforehand. A schematic of the configuration is presented in Fig. 4. If this distance is *s*, it must be related to the other variables in the problem using a triangle whose three apices are the origin of the window-centered system W, the origin of the sphere S and the arbitrary point on the internal wall, P, and then the whole system solved using the Law of Cosines for spherical triangles and the Law of Sines and of Cosines for planar triangles.

The given quantities are α and β, the window-centered zenith and azimuth angles to the previously-mentioned P, the given triplet (a,b,c), the window-centered Cartesian location of the sphere center (computed by differencing the coordinates of the sphere center and the window centers, both in SH coordinates) and R, the radius of the sphere. These quantities determine the intermediate values Δ, α_0 and β_0,

$$\Delta = \sqrt{a^2 + b^2 + c^2}$$
$$\alpha_0 = \cos^{-1}(c/\Delta)$$
$$\beta_0 = \tan^{-1}(b/a)$$

which fix ρ, the value of the angle PWS, by the Law of Cosines for spherical geometry

$$\cos\rho = \cos\alpha\cos\alpha_0 + \sin\alpha\sin\alpha_0\cos(\beta - \beta_0).$$

The Law of Sines and of Cosines for planar geometry then gives the length *s* from the window center to P:

$$s = \sqrt{\Delta^2 + R^2 - 2\Delta^2 \sin^2 \rho + 2\Delta \cos \rho \sqrt{R^2 - \Delta^2 \sin^2 \rho}} \ .$$

Knowing a and b, the window-centered zenith and azimuth angles, the (x,y,z) location of P in the window-centered system becomes

$$\begin{aligned} x &= s \sin\alpha \cos\beta - a \\ y &= s \sin\alpha \sin\beta - b \\ z &= s \cos\alpha - c \end{aligned}$$

Computing the azimuth and zenith angles of P becomes a question of applying the window-centered to sphere-centered transformation,

$$\begin{aligned} x &= -y \\ y &= x \\ z &= z \end{aligned}$$

and then converting Cartesian to spherical coordinates:

$$\begin{aligned} \phi &= \tan^{-1}\left(\frac{y}{x}\right) \\ \theta &= \cos^{-1}\left(\frac{z}{R}\right) \end{aligned} .$$

These are the x and y axes of the plots in Appendix B.

Solar Aureole Window Centers

An added complication must be factored in when considering the four windows of the solar aureole monochromatic polarizing low-resolution cameras. The window center coordinates cited in Lockheed-Martin-dimensioned drawings of the front of the SH are $(x,y,z)_{SH}$=(37.020,42.949,204.747) mm. Relative to the window center and a coordinate system aligned to the plate holding the 4 Solar Aureole windows, the locations of each window are given by

$$\vec{x}_{SA1} = \begin{pmatrix} 8.30 \\ 0 \\ 0 \end{pmatrix}$$

$$\vec{x}_{SA2} = \begin{pmatrix} 2.75 \\ 0 \\ 0 \end{pmatrix}$$

$$\vec{x}_{SA3} = \begin{pmatrix} -2.75 \\ 0 \\ 0 \end{pmatrix}$$

$$\vec{x}_{SA4} = \begin{pmatrix} -8.30 \\ 0 \\ 0 \end{pmatrix}$$

where the x-axis is aligned vertically with the plate, the z-axis perpendicular to the plate along the optical axis and pointing toward the sky and the y-axis perpendicular to both in a right-handed system.

Rotating these coordinates back to the SH system by –6° around x and –40° around y and then adding the plate center's own dimensions gives the SA 1, 2, 3 and 4 coordinates listed in Table 1, the table of window centers above.

Monochromator Window Center

Another complication is provided by the monochromator. It sits at a port located at a CCW angle of 300° from the DISR SH, which places it 60° towards the left side as seen from the SH (clockwise). The monochromator points toward a location on the equator of the inner wall of the sphere 180° away. This spot is nominally located at a spherical azimuth of 120°. It is an F/4 monochromator with an entrance slit 5 mm wide by 20 mm long. The speed of the system determines the acceptance angle for light from the integrating sphere wall (which is not focused or filtered in any way, but simply shines directly into the slit). Thus, the "field of view", or area of sensitivity, of the monochromator system on the integrating sphere wall is a disk approximately 14° in diameter. The disk is slightly elongated along the long axis of the slit (zenithally in the integrating sphere coordinate system).

The complication comes because the monochromator's window-centered coordinate system is not aligned with that of the other window-centered systems, the integrating-sphere system, or the DISR SH system. This requires a coordinate rotation around the z-axis of the window-based system in order to convert the origin of the sphere's coordinates from nominal DISR SH window-based coordinates to monochromator window-based coordinates. Then it requires an inverse transformation from monochromator window-based coordinates to the nominal DISR window-based coordinates.

Appendix A: The Private Life of an Integrating Sphere: the Radiant Homogeneity of the DISR Calibration Sphere

Abstract

A 50-cm-diameter integrating sphere's radiant uniformity is mapped when the 200-cm^2 optical system being calibrated protrudes into the interior. The Descent Imager/Spectral Radiometer (DISR) contains subsystems looking upward and downward, some with large fields of view. Inserting the DISR Sensor Head (SH) into the calibration sphere provides a practical platform for many of the calibrations, but the resulting non-uniformity threatens the goal of 1% radiometry. An apparatus is built to measure the radiance variations. It finds the radiance field to be homogeneous over most of the sphere to the level of 1-2%, with large excursions near the SH, away from its subsystems' fields of view.

Introduction

Radiometric calibration of flight instruments using an integrating sphere of moderate diameter fulfills several key engineering requirements. Such a sphere mounts easily to an optical table and permits the convenient attachment of detectors and sources. It can be sealed and purged with dry air, allowing instruments connected to it to attain temperatures far below ambient. It completely fills the field of view of adjoining optical systems with bright, diffuse and homogeneous radiance. How homogeneous is the subject of this paper.

This work measures the extent to which a sphere's uniformity is disrupted when the primary optical system being calibrated protrudes significantly into its interior. It reports a mapping of the spatial homogeneity, or flatness, of the inside surface of a 50-cm integrating sphere characterizing a specific optical system. Previous work has studied larger spheres and less intrusion into the spherical cavity[1].

This system is the Descent Imager / Spectral Radiometer (DISR), the only optical instrument on the Huygens Probe of the Cassini mission to Saturn[2]. In November 2004, this probe will be directed into the atmosphere of Titan, Saturn's largest moon, and DISR will become the first camera to view Titan's lower atmosphere and surface from within the atmosphere and from below the haze layer which shrouds the satellite from more remote observation. It will measure upward- and downward-streaming fluxes of light all the way through the atmosphere in the UV, visible and near-IR spectral ranges and use this data to derive an altitudinal profile of the radiative forcing of Titan's atmosphere.

To the DISR cameras, spectrometers and photometers, a large integrating sphere provides: 1) a homogeneous, Lambertian surface for flat-fielding the imagers, 2) a spectrally featureless reflectance curve useful in characterizing the spectral responsivity of the imagers and spectrometers, 3) an enclosure easily purged with dry nitrogen that permits detector focal planes to be cooled to their field temperatures during measurements of absolute responsivity, 4) a surface homogeneous and Lambertian enough that its absolute brightness can be faithfully calibrated by standard detectors and auxiliary detectors and 5) an ability to accommodate optical systems with wide fields of view.

DISR is far from being the only optical system to take advantage of the properties above. The unique spatial uniformity and brightness of their internal surfaces make integrating spheres a frequent choice for radiometric transfer. Usually, though, the instrument being calibrated views the interior wall of the sphere from outside the sphere's metal shell. The wall brightness of a typical integrating sphere outside the first bounce region is uniform to a high order when the sphere is illuminated and observed through

ports that lie flush to the sphere's surface. This is strictly true when there are no structures inside that occupy the sphere's internal volume as opposed to representing a two-dimensional area on the inside wall surface.

Calibrating DISR with the sphere violates this condition. Its sensor head (SH) is inserted *into* the calibration sphere, as shown in Fig. A-1. The front

Figure A-1

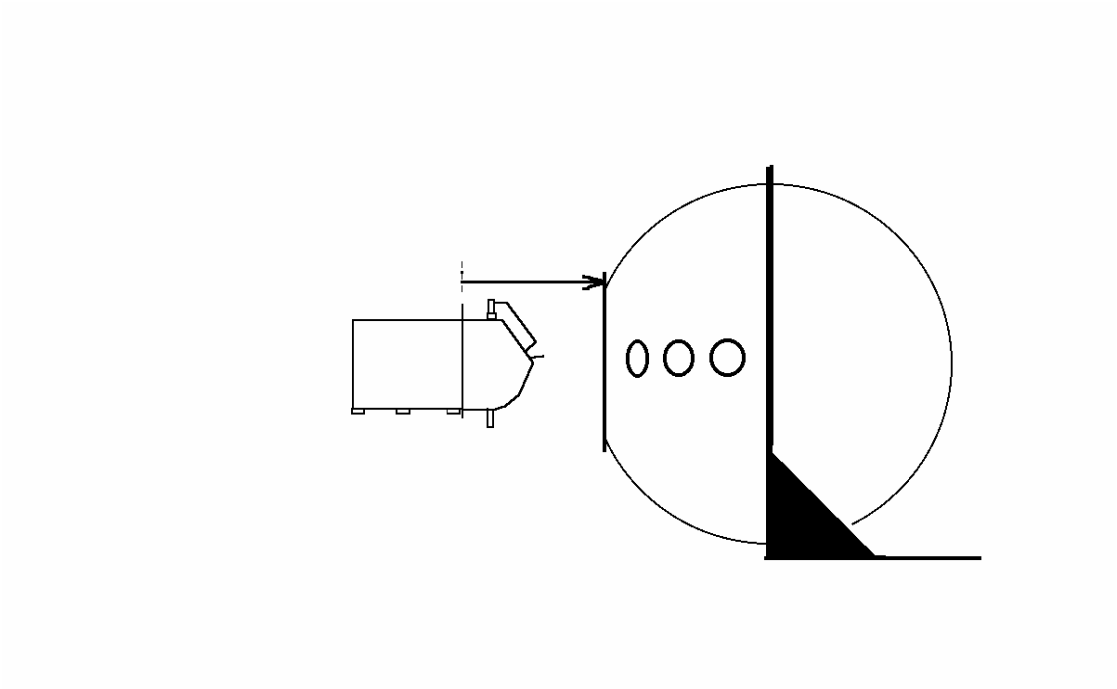

housing of the SH possesses a cross-section of 10 by 12.5 cm and protrudes some 9 cm into the interior of the sphere. The SH front housing, which is covered in a textured black foam, sports asymmetrically-placed protrusions: three bear's-ear baffles, a shadow bar and a sunshade for one of the imagers. The asymmetry of this black lopped-off columnar object tends to spoil the uniformity of a spherical surface radiance normally achieved by the joint operation of angle-independent scattering, projected surface area and the inverse-square law.

Models constructed of the internal brightness variations within the sphere given the size and approximate shape of DISR at the central port show that variations on the front wall, the side opposite and furthest away from the DISR SH, would be of the order of a 1-2 %, increasing toward the SH itself. Since the goal throughout the DISR calibration is 1% relative accuracy and since the fields of view of several of the sub-instruments include the front half of the sphere, a more experimentally based characterization is desired.

An apparatus is built to quantify the radiance variations. A radiance map of the inside of the sphere is derived from data mapping the brightness variations of the interior wall. The discussion below begins with a review of relevant details of the DISR instruments, includes a brief discussion of the theoretical basis for a sphere's uniformity, describes the apparatus used to gather the brightness data, reports on the data's analysis and interpretation and concludes.

DISR and its Calibration

Mounted on a spinning platform that will descend to the surface of Titan by parachute, DISR gathers the light it measures through several separate light paths. They are summarized in Table 1.

Table A-2

Instrument	Pointing (Azimuth, Zenith) (deg)	Azimuth x Zenith Range (deg)	Wavelength (nm) and/or Polarization
Upward-Looking Violet Photometer (ULV)	(0,0)	170 x 83	350-480
Upward-Looking Visible Spectrometer (ULVS)	(0,0)	170 x 83	480-960
Upward-Looking Infrared Spectrometer (ULIS)	(0,0)	170 x 83	870-1700
Solar Aureole 1	(-6,50)	6 x 50	500, parallel
Solar Aureole 2	(-6,50)	6 x 50	500, perp.
Solar Aureole 3	(-6,50)	6 x 50	930, parallel
Solar Aureole 4	(-6,50)	6 x 50	930, perp.
Sun Sensor	(0,50)	64 x 50	940
Downward-Looking Violet Photometer (DLV)	(0,180)	170 x 83	350-480
Downward-Looking Visible Spectreometer (DLVS)	(0,150)	4 x 40	480-960
Downward-Looking Infrared Spectrometer (DLIS)	(0,160)	3 x 9	870-1700
High-Resolution Imager (HRI)	(0,166)	9.6 x 15.2	660-1100
Medium-Resolution Imager (MRI)	(0,149)	21.1 x 30.5	660-1100
Side-Looking Imager (SLI)	(0,109.4)	25.6 x 50.8	660-1100

Three broadband imagers record panoramas from near-nadir to above the horizon. Four wide-field low-resolution cameras image the sky's brightness at many solar zenith angles in the near-IR and green, at 2 orthogonal polarizations. Of four spectrometers, two look upward and two downward, and cover the spectral region from 0.48 to 1.7 μm. The upward spectrometers gather light over almost half the upper hemisphere through horizontal diffusers. Two broadband photometers in the near ultraviolet collect light through diffusers from both the upward and downward directions. A picture of the sensor head from above and below is displayed in Figure A-2.

Figure A-2

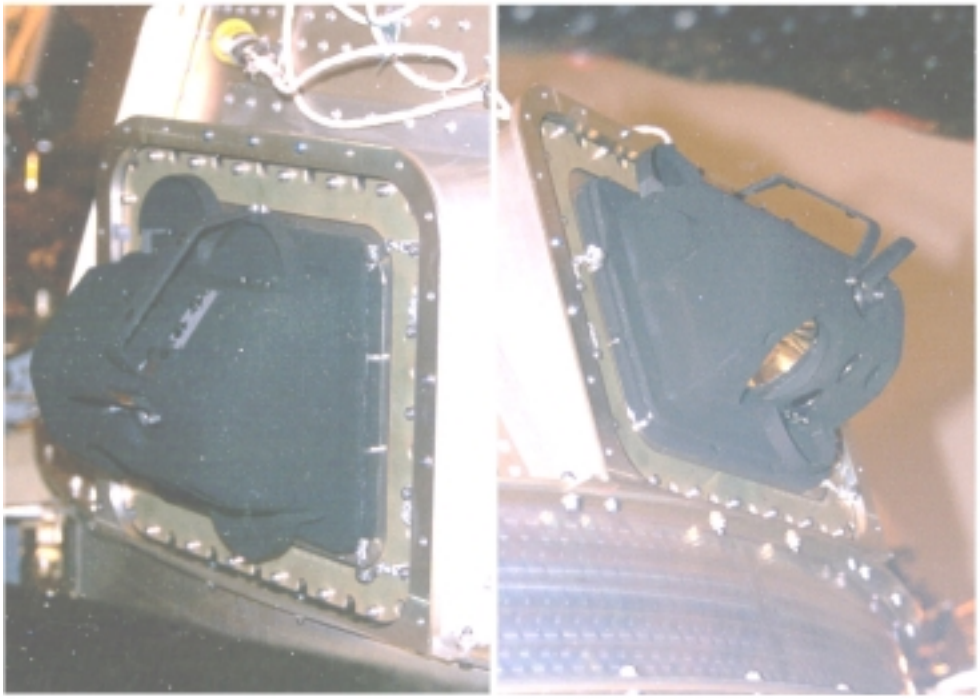

The photographs indicate the general shape of the sensor head (SH) and show the various structures attached to its front housing: the 3 hemispherical bear's-ear baffles, the sunshade protruding from the front nose of the SH and the shadow bar. The exterior is coated with thermally shielding foam painted flat black.

DISR has several distinctive optical features. It brings along its own 20W light source, which points downward toward Titan's surface and illuminates the ground in the final few hundred meters of the descent. It supports the shadow bar, which blocks the solar direct beam from several of the upward-looking instruments. A wide-angle, sun-sensing photometer, looking upward through 3 reticles arrayed in a splayed configuration, provides an azimuth zero at every rotation based on the detection of a triplet of pulses from the Sun. Coherent fiber optic cables conduct the light collected by various foreoptics to two glass conduits which then convey it to the main detectors: a Si CCD array and two InGaAs linear CCDs. Finally, the light from a trio of single-watt lamps can be injected into the optical systems of each of the DISR instruments, providing a common internal calibration.

Calibration of the DISR, besides measuring absolute responsivity, also includes spectral and spatial responsivity, point spread function, cross talk, out-of-field response, direction, pixel field angles, polarization sensitivity, linearity, wavelength and spectral point spread function. Absolute and spectral responsivity is measured as a function of temperature.

Two qualitatively different test stations conduct most of DISR's calibrations. An altitude-azimuth mount positions and orients the DISR toward various sources and targets in order to measure spatial and polarization responsivity, point spread function, distortion, direction and pixel field angles. But the balance of the tests, including absolute and spectral responsivity, linearity, wavelength, spectral point spread function calibration and the dependence of responsivity on temperature rely on covering the DISR sensor head's front housing with an integrating sphere.

An Integrating Sphere's Uniformity

It is useful to briefly review the theoretical basis for an integrating sphere's homogeneity. More extensive theoretical discussions can be found elsewhere[3,4].

The integrating sphere, supplied by Labsphere, measures 50 cm in diameter with one section removed to create a main port with a diameter of 20 cm. Its interior is coated with Spectraflect, Labsphere's barium sulfate textured surface. Six 5-cm ports are mounted on the sphere's equatorial plane, three to each side of the large central port, making a total of 7 ports. The ports are numbered from 1 to 7 starting with the leftmost port as viewed from the point of view of the SH and moving counterclockwise. The location and use of each port is outlined in Table 2. Azimuths increase from 0° at the main port to 180° on the front wall. Unused ports are capped with port covers internally coated with material identical to that coating the bulk of the sphere.

Table A-3

Port	Azimuth	Instrument		
1	282.5	Reference Detectors		
2	300	Monochromator		
3	317.5	Unused		
4	0	DISR Dummy Sensor Head		
5	37.5	Lamp Injection Baffle		
6	53.5	Unused		
7	77.5	Unused		

Photons enter the sphere at port 5. They are largely removed by being absorbed either by the surface of the SH or at one of the ports where monitoring or calibrating detectors are positioned. Only absorption at a port preserves the homogeneity of the sphere wall's radiance. Both entry and absorption on the SH's surface contribute to non-uniformity in the radiance, as is well known for integrating spheres.

First-bounce regions of brightness or auxiliary detector port regions of darkness confined to the inside surface of an integrating sphere wall will donate an identical irradiance to any arbitrary point of the sphere due to the Lambertian nature of the sphere coating and the spherical morphology of its shell. As long as these structures do not protrude into the internal 3-space of the sphere then any arbitrary point on the internal wall will receive exactly the same irradiance from each structure.

To see this, refer to Fig. A-3. Assume that an arbitrary bright or dark region,

Figure A-3

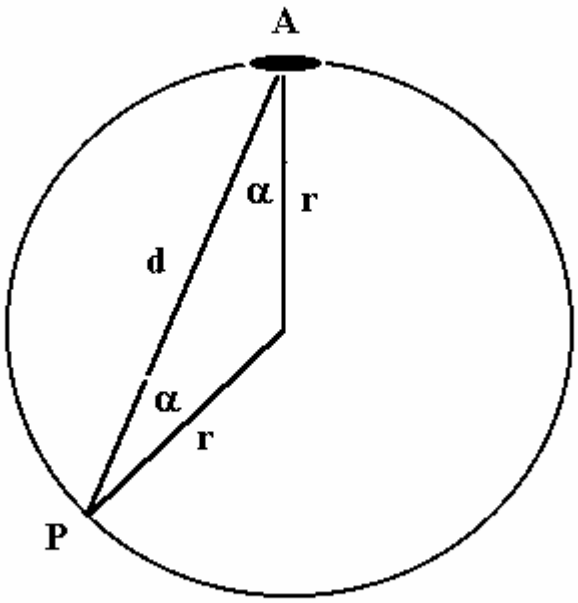

labeled A, on the inside surface of the sphere, possesses area *a* and is Lambertian. Express the irradiance, *E*, at an arbitrary point P on the sphere wall, also Lambertian, from the direction of A as the product of A's radiance, *L*, and the projected solid angle, Ω, it subtends from P, oriented at angle α to the normal,

$$E = L\Omega \tag{1}$$

All quantities are assumed to apply at a specific wavelength λ. The radiance emerging from P, which is denoted *l*, is the sum of the irradiances from all *n* regions, A_i, of light and darkness on the sphere wall subtending nonzero projected solid angle as seen from P, multiplied by the wall's reflectance at P, denoted ρ, and divided by π, the solid angle into which light from P radiates:

$$l = (\rho / \pi)(E_1 + E_2 + ... + E_n) \tag{2}$$

Referring to Fig. A-3, we express Ω in terms of 1) *a*, the area of A, 2) α, the angle between A's normal and the chord AP, 3) the angle between P's normal and AP, also equal to α because of the spherical geometry, and 4) *r*, the radius of the sphere. The intermediate quantity *d* is the length of AP.

$$\Omega = \frac{A\cos\alpha\cos\alpha}{d^2} = \frac{A\cos^2\alpha}{d^2} = \frac{A\cos^2\alpha}{4r^2\cos^2\alpha} = \frac{A}{4r^2} \tag{3}$$

The radiances at any number of points P_i on a sphere's internal wall whose fields of view include the Lambertian regions A_i, also on the surface of the sphere, will therefore be equal to a quantity which does not depend on position α, but only on parameters characterizing the whole sphere. The radiance anywhere inside the sphere not located within the A_i is therefore constant and the radiation field homogeneous.

But when an object is actually inserted into the ball-shaped volume of the sphere, then the assumptions underlying the above result are violated. P's radiance will differ from that at other points to the extent that A's solid angle from different vantage points on the wall differs from cosine dependence. P's radiance will then depend on its placement with respect to the volume protruding into the interior ball. For example, if the protruding object A is ball-shaped and if P is located by the angles θ and ϕ, the co-latitude and azimuth angle of a spherical coordinate system whose North Pole is the center of the port containing the protruding ball, then it can be shown that the solid angle Ω of A as seen from P at θ and ϕ, is given by

$$\Omega = \frac{\pi R^2 (1 + \theta / \pi)}{8 r^2 \sin(\theta / 2)} \tag{4}$$

where R is the radius of A, an expression that depends on the location of the point within the sphere, θ, though not on ϕ, because of the spherical symmetry

The DISR sensor head, unlike the ball in the above example, is not spherically symmetric. Assessing its effect on the uniformity of the integrating sphere's radiance is more difficult. Two approaches are followed. First, an attempt is made to compute theoretically the dependence of radiance as a function of location on the sphere's interior wall, an effort not discussed in this paper. Second, an apparatus is constructed to measure this dependence. It will now be described.

Apparatus

The apparatus used to characterize the internal radiance of DISR's calibration sphere is shown in Fig. A-4. It consists of 5 main parts: 1) a metal shell, called the dummy sensor head (DSH), covered in the same foam and black paint and possessing the same external dimensions as the actual sensor head except for a circular 5-cm-diameter cavity at the front, voluminous enough to accommodate a fork-mounted turret assembly, 2) the turret assembly itself, capable of pointing a brass tube at different angles from the central axis of the integrating sphere, 3) a broadband Si photodiode mounted within the brass tube in front of a lens, 4) another, and much longer, brass tube aligned with the central axis penetrating the DSH's cover plate and connecting to a perpendicular adjusting arm capable of positioning the fork assembly at different angles around the central axis and 5) a cover plate that serves as the DSH's mounting interface to the sphere itself as well as locating and locking the adjusting arm at different angles.

Figure A-4

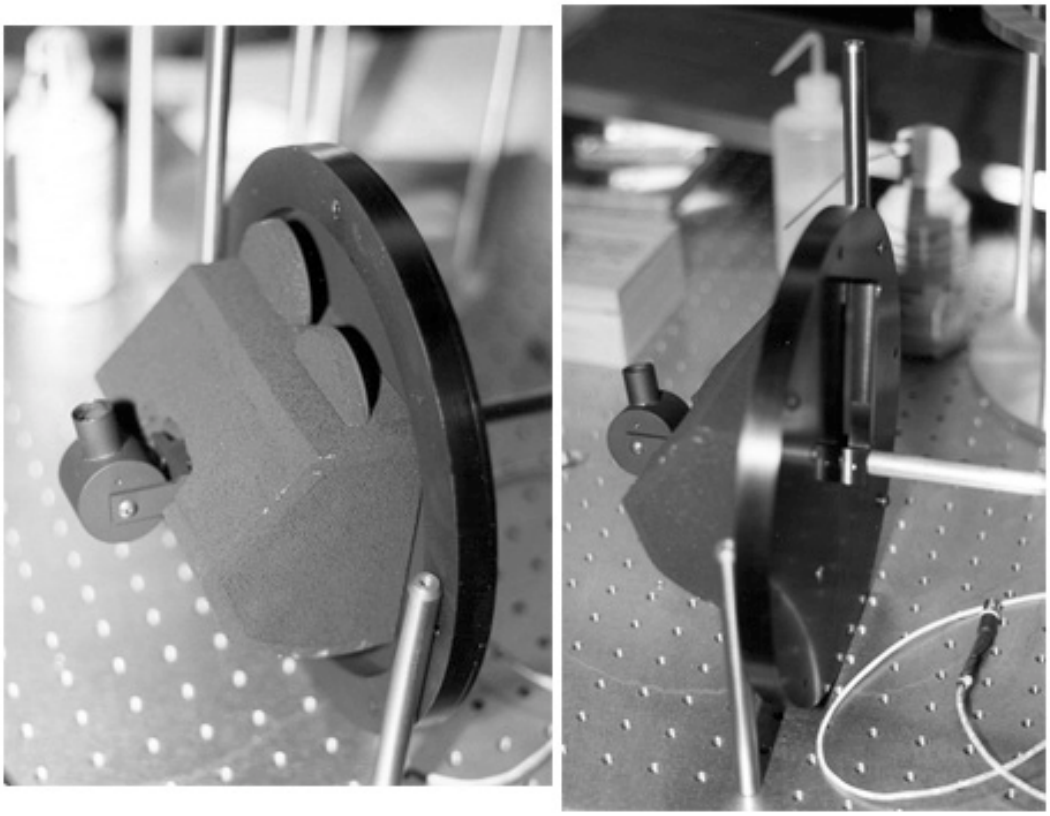

The central and auxiliary ports of the integrating sphere are all positioned on the sphere's equator. All dark and first-bounce bright regions of the sphere (labeled A_i in the previous section) are thus confined to the equator by design. The entrance windows of DISR's various instruments are mounted on the front of the sensor head and look upward and downward but none of them, except for the Side-Looking Imager (SLI), include the equatorial region of the integrating sphere within their field of view. The SLI looks toward the front of the integrating sphere (ϕ=180°), expected to be the most uniform region of the sphere.

The port arrangement is summarized above in Table 2. Attached to the ports of the integrating sphere are the broadband lamp source at port 5 and a triplet of auxiliary detectors at port 1. At port 2, a monochromator is mounted in a configuration identical to that of several DISR calibrations, but it otherwise has no data-collection function during the homogeneity measurement and does enter into this discussion.

At port 1, mounted behind a diffuser in a common thermal block is a triplet of 3 detectors: an EG & G UV-245BG Si photodiode used in a broadband configuration, an identical UV-245BG Si photodiode filtered by a 100-nm wide band pass filter centered at 430 nm, and an EPITAXX ETX 3000T5 InGaAs photodiode (responding from 0.8 to 1.7 μm) used in a broadband mode. The temperature of the detector block is stabilized to a temperature just a few degrees above room temperature by resistive heaters. Of these 3 auxiliary detectors, the broadband Si photodiode monitors the general level of luminance inside the integrating sphere. It provides a temporal reference for an identical detector mounted in the turret, under the expectation that fluctuations in QTH lamp output cause variations in the average radiance. It is estimated that an additional source of variation in the radiant uniformity: the changing geometry of the DSH and its solid angle Ω caused by the movement of the turret in its fork mount through the two-

degree-of-freedom range, introduces little additional error; however, the auxiliary detectors also monitor this variation and are used to correct it. The turret detector used to gather the homogeneity data is an EG & G UV-245BG Si photodiode used broadband, identical to the Si broadband detector used in the auxiliary triplet of detectors mounted at port 1.

At port 5, the source of light for the integrating sphere is a condensing-focusing system fed by a 150 W broadband quartz-tungsten-halogen (QTH) bulb. The beam of light is directed at a baffle mounted 5 cm within the integrating sphere aligned to the port. The baffle is positioned at an angle of 45° to the normal of the port, so as to direct first-bounce light toward the back of the integrating sphere, i.e., the side where the DISR sensor head or DSH is mounted. The QTH source is shuttered.

The spatial homogeneity apparatus achieves a general pointing accuracy of a few tenths of a degree. The field of view of the detector-lens configuration possesses a full width at half-max responsivity of some 10°. The center of rotation of the two-axis system is located at a distance of 8.6 cm from the edge of the sphere along the central axis, running normal to the large central port. The back of the sphere is defined to be the side containing the large central port; the front of the sphere the side toward which the DISR sensor head and dummy sensor head look.

The angles α and β that characterize the different positions of the fork mount turret assembly are defined in Fig. A-5. The detector fork mount assembly

Figure A-5

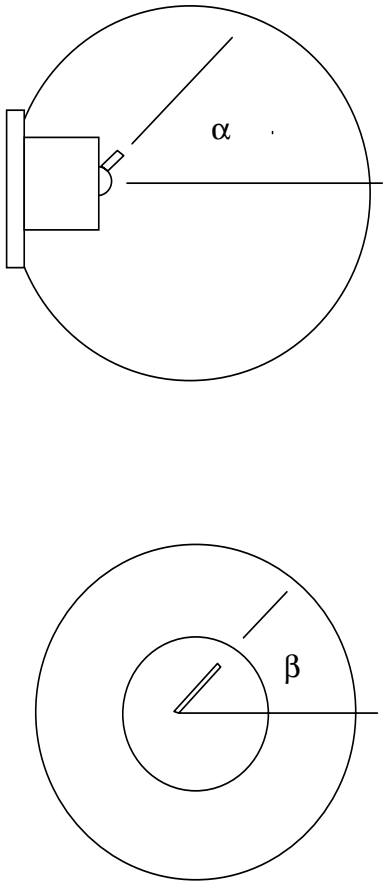

is manually rotated about the central axis by the experimenter using an adjustment arm. The hollow brass tube, 20 cm long, 1.7 cm in diameter, that penetrates the 20-cm-diameter cover plate and connects the adjusting arm to the fork mount assembly, also guides the wires conducting the detector signal to a connector outside the integrating sphere. The adjusting arm can be placed at any angle and can be locked into position at any one of 36 detent positions, spaced at 10° intervals to within 0.1°. The fork mount assembly rotates about an axis perpendicular to the central axis of the sphere to orient the 5-cm brass tube that contains the detector and lens assembly, to different angles with respect to the central axis. As with the cover plate and adjusting arm, detents are accurately placed at 10° intervals on the body of the fork assembly turret, allowing the detector barrel to be locked into positions from straight ahead ($\alpha = 0°$) to $\alpha = 110°$, which points the barrel toward the rear of the integrating sphere, but not all the way to the axis.

The turret is prevented from turning to examine the dummy sensor head (DSH) by the DSH's own shell.

Data Acquisition and Analysis

The data consists of some 5300 turret and simultaneous auxiliary-Si detector signals that are mediated by similar transimpedance amplifying circuits digitized and recorded using a computer interface. A total of 316 distinct directions within the sphere are sampled, each with α between 0 and 110° in 10° increments and β between 0 and 360° at increments in multiples of 10°. Measurements at each direction are performed in sets of 10 and then averaged. The pointing angles of the fork mount detector assembly are chosen to achieve as uniform a density of points as possible. The points at which measurements are made are indicated on the Mercator projection summarizing the results in Figure A-6.

The 150 W QTH FDS broadband source illuminating the integrating sphere during the measurements is identical in characteristics and injection geometry to lamps used during DISR absolute calibrations and flat-fielding. The lamps are driven at their design current of 6.25 A. At this current they typically last 100 hours. The lamp used has been run for 5 hours when the measurements begin and is then used for 22 hours. It is powered by an Optronic Labs OL-65S DC supply.

At each point on the interior surface of the integrating sphere, ten bright (shutter open) detector readings are recorded in a group at a specific α and β setting before the adjusting arm is moved to a new β setting. At the end of the group of β settings, the port cover is unmounted from the integrating sphere and the fork mount assembly moved to a new α setting. At the beginning and end of each circle of β readings, a group of 4 dark (shutter closed) measurements is recorded.

All turret and auxiliary-Si signals are dark-subtracted by an average of the most nearly coincident darks and then the turret readings divided by the simultaneous auxiliary-Si signals to take out variations in the general brightness level inside the sphere due to lamp fluctuations and geometry shifts. The normalized signals are transformed from the apparatus' (α,β) system to a sphere-centered (θ,ϕ) Mercator system using the following relations:

$$
\begin{aligned}
x &= \left[r^2 - (r-d)^2 \sin^2\alpha\right]^{1/2} \cos\alpha + (r-d)\sin^2\alpha \\
y &= \left[r^2 - (r-d)^2 \sin^2\alpha\right]^{1/2} \sin\alpha\cos\beta - \cos\alpha(r-d)\sin\alpha\cos\beta \\
z &= \left[r^2 - (r-d)^2 \sin^2\alpha\right]^{1/2} \sin\alpha\sin\beta - \cos\alpha(r-d)\sin\alpha\sin\beta \\
\theta &= \cos^{-1}\left(\frac{z}{r}\right) \\
\phi &= \tan^{-1}\left(\frac{y}{x}\right)
\end{aligned}
\qquad (5)
$$

where r is the radius of the sphere and d is the offset along the central axis of the pivot point for the fork-mounted turret. In the sphere-centered system the back center of the sphere, where the DISR Sensor Head (SH) is located, is at θ=90°, ϕ=0°, the front center is at θ=90°, ϕ=180°, the top is at θ=0° and the bottom is at θ=180°.

The percentage difference between a typical normalized signal and the average of those at the sphere's front-center is computed. The resulting isophotic contour is displayed in Fig. A-6. Each contour line is labeled with the

Figure A-6

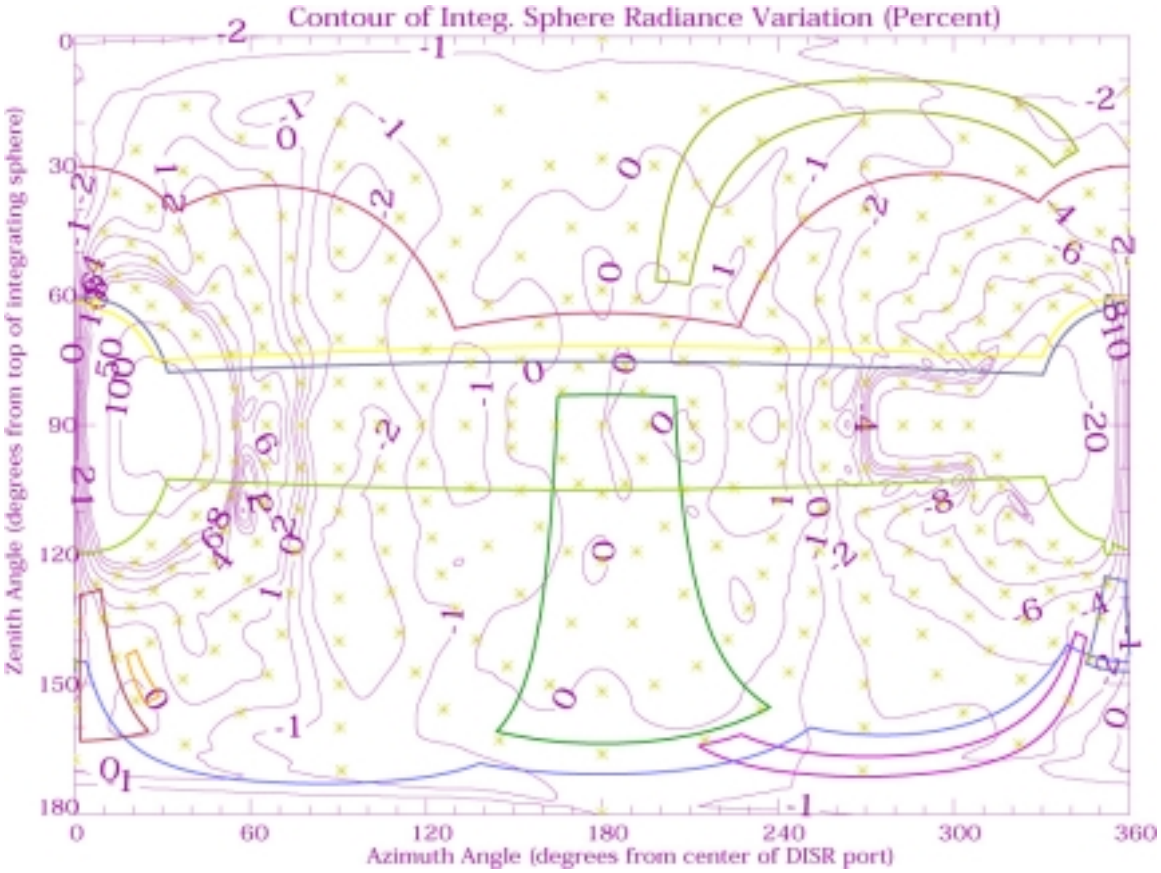

percentage deviation in brightness from the front center of the sphere, where the deviation is defined to be zero. Positive deviations represent brighter regions. Also displayed are the 316 points where measurements occur, denoted by asterisks, and the outlines of the fields of view of the various DISR instruments. Refer to Table 1 for the specifications of the pointing and fields of view of the various DISR instruments.

The data presented in Fig. A-6 is used to construct a gray-scale image of the inside of the DISR calibration sphere as seen in a piecewise fashion by the DSH apparatus. It is displayed in Fig. A-7.

Figure A-7

The derived brightness varies at the resolution of the 10°-wide detector-sampling region. As can be seen from Fig. A-6, the scale of significant variations in integrating sphere brightness over the front half of the sphere is found to be significantly larger than the sampling area of the detector, indicating that the general results are largely independent of the detector sampling area.

The main correctable sources of error in the measurement are 1) drift in the lamp, 2) the changing geometry of the fork-mounted turret assembly as the angle β is varied around a full circle, and 3) the changing geometry of the fork-mounted turret assembly as the angle α is varied through its range. All of these effects are essentially corrected by dividing by the reference Si detector measurements. A minor source of error, the non-zero settling time of the detector and differences in brightness caused by readings occurring at different relative times, is reduced to a negligible magnitude by averaging each set of 10 measurements. The integrated brightness of the integrating sphere drifts by ~3% over the 22-hour period over which measurements are recorded, as determined by the auxiliary-Si detector. The brightness variation over a full cycle of the angle β is typically ~0.7%.

The major uncorrectable error in the isophotic contours displayed in Fig. A-6 is caused by the extent to which the exact shape of the dummy sensor head differs from that of the DISR sensor head as viewed from various points on the sphere's interior. The main morphological dissimilarity is the existence of the fork turret on the front of the dummy sensor head. The cross-section of the fork turret is some 15 cm^2, compared to the typical 155-cm^2 front cross-section of the sensor head's main structure or to its 61-cm^2-side cross-section. The error is basically negligible on the front-wall, where the turret's cross-section is lost against the larger solid angle of the sensor head. It begins to become

noticeable starting at points more than about 75° away from the front-center of the sphere, where the turret can be seen as a silhouette protruding outward from the front of the sensor head. Toward the side, top and back of the sphere, the error incurred at these locations may approach 25 % of the recorded relative brightness deviations. In between the error is generally of the order of 10 %. In any case, it is an unavoidable error, correctable only by modeling the sphere's internal brightness in a detailed fashion, something that will not be treated in this work.

Discussion

As Fig. A-6 implies, most of the variation in relative radiance over the area of the integrating sphere seems to be related to three effects: 1) the location of a point either within a dark region such as the ports where auxiliary detectors, the monochromator or the DISR itself is mounted, 2) the location of a point within the bright first-bounce region of the lamp injection port and baffle or 3) the proximity of a point to the region of the DISR sensor head at port 4 and the injection baffle at port 5. The degree of variation is highly nonlinear: very little variation is seen over a wide range for distant points, while much more rapid variation is seen for points near the SH. The first and second effects would hold true for any integrating sphere with dark or bright regions. The third effect holds because of the existence of the DISR SH within the volume of the sphere. The shape and magnitude of its solid angle for nearby points versus distant ones does follow the cosine dependence necessary to achieve a uniform field. The source injection baffle also contributes to the nonhomogeneity though to much less a degree.

The variation in brightness over the integrating sphere's front surface is minor, attaining a maximum of +2 and a minimum of -2 %, both located near the equator and thus out of the field-of-view of most DISR instruments. The asymmetry of the radiance profile reflects the change in the shape of the dummy sensor head, especially the shadow bar, as seen from those two locations. Within the fields of view of most of the DISR instruments, the variation is 1-2% and only at the edges of the hemispherical instruments does this increase to 6-8 %. Even in the downward-looking instruments whose fields of view are right under port 4, the variation from the front of the sphere is no more than 2-3 %.

Much of the brightness variation within the sphere occurs on the equator, where all of the ports are located, where the light is injected and where the main absorbing surface -- DISR itself -- is positioned. This aspect of the brightness variation is achieved by confining the ports to the equator of the back half of the sphere. Most of the DISR's instruments do not look at the equator; the only instrument whose field of view includes the equator--the SLI--looks only at the front half of the sphere, where the variation is slightest.

Conclusion

An integrating sphere of moderate size used for radiometric calibration provides an internal radiance field flat to 2 % over much of the interior even when the primary optical system being calibrated possesses a substantial surface area and protrudes significantly into its interior. Even an instrument with unusually extensive fields of view, both upward and downward, is able to assume the sphere's internal radiance field to be uniform. When coupled with an internal map of the sphere's deviations from uniformity, a goal of relative errors less than or equal to 1 % can be achieved.

As might be expected, significant variations from homogeneity, in addition to the first-bounce regions of light and darkness, occur near the objects that protrude into the sphere's internal volume. At larger distances, the three-dimensional relief associated with these objects is not as detectable and the object's cross-section from one point is similar from many points of view. This explains the lack of relative brightness variation of the sphere's front wall as measured in this work.

Figure Captions

1. Schematic showing the relative size, orientation and placement of the DISR sensor head with respect to the 50-cm-diameter integrating sphere used as the test station for performing many of the calibrations.

2. The DISR Sensor Head seen from above and below, attached to the Huygens Probe.

3. Diagram displaying the geometry relating a dark or bright first-bounce region A and an arbitrary point P on the sphere's interior wall. The various angles and line segments are labeled.

4. Photographs depicting the dummy sensor head (DSH), the apparatus used to measure the spatial dependence of radiance on location within the DISR calibration sphere. The various components of the assembly are described in the text.

5. Schematic defining the angles α and β.

6. Spatial radiance profile of the interior of the DISR calibration sphere subject to the absorbing region of the Dummy sensor head (DSH). An accurate approximation to the spatial radiance map when the DSH is replaced by the actual DISR sensor head. Relative brightness contours, or isophotes, are marked in % deviation relative to the front-center of the integrating sphere. The locations of the actual measurements are marked with asterisks. The boundaries of the fields of view of the various DISR instruments are indicated.

7. Image constructed of the inside of the 50-cm-diameter DISR calibration sphere derived from the spatial radiance map based on the Dummy sensor head (DSH).

References

1. W.A. Hovis and J.S. Knoll. "Characteristics of an internally illuminated calibration sphere." *Appl. Opt.* **22**, 4004-4007 (1983).

2. M.G. Tomasko, D. Buchhauser, M. Bushroe, L.E. Dafoe, L.R. Doose, A. Eibl, C. Fellows, E. McFarlane, G.M. Prout, M.J. Pringle, B. Rizk, C. See, P.H. Smith and K. Tsetsenekos, "The Descent Imager/Spectral Radiometer (DISR) experiment on the Huygens entry probe of Titan," to be published in *Sp. Sci. Rev.* (2000).

3. D.G. Goebel, "Generalized integrating-sphere theory," *Appl. Opt*. **6**, 125-128 (1967).

4. A.C. Hardy and O.W. Pineo. "The errors due to the finite size of holes and sample in integrating spheres." *J. Opt. Soc. Am.* **21**, 502-506 (1931).

Appendix B: Integrating Sphere Relative Brightness as Seen from Instruments

The maps of relative brightness shown in this section are produced from the tables listed in Appendix C. They are presented on a grid of window-centered azimuth and zenith angle. The azimuth angles run from 0^o on the right-hand side to 180^o on the left-hand side; the zenith angles run from 0^o on the top to 180^o on the bottom. Such an extent more than covers the internal walls of the integrating sphere as seen by any of the DISR instruments or the laboratory monochromator, the detector system used to transfer the absolute radiance standard to the radiance of the walls of the integrating sphere and therefore to all of the DISR instruments.

The units of the relative brightness contours are % deviation from the front-center point of the sphere ($\phi=180^o$, $\theta=90^o$ in the sphere-centered coordinate system), where the relative brightness is defined to be 0 %. Positive relative brightnesses are areas brighter than the front center of the sphere; negative ones are darker areas.

Nominal outlines of DISR's instrument field of view are overlaid as solid black lines on the contour lines of the relative brightness measurements. In all cases, the actual spatial responsivity of each of the instruments is more complicated and correctly represented by the calibrated spatial responsivities, which are not shown here. The correct accounting of the relative brightness of the light actually seen by an instrument inside the integrating sphere is correctly produced by multiplying the relative brightness in these maps with the spatial responsivities and then spatially integrating or not, as required by the instrument's own modality.

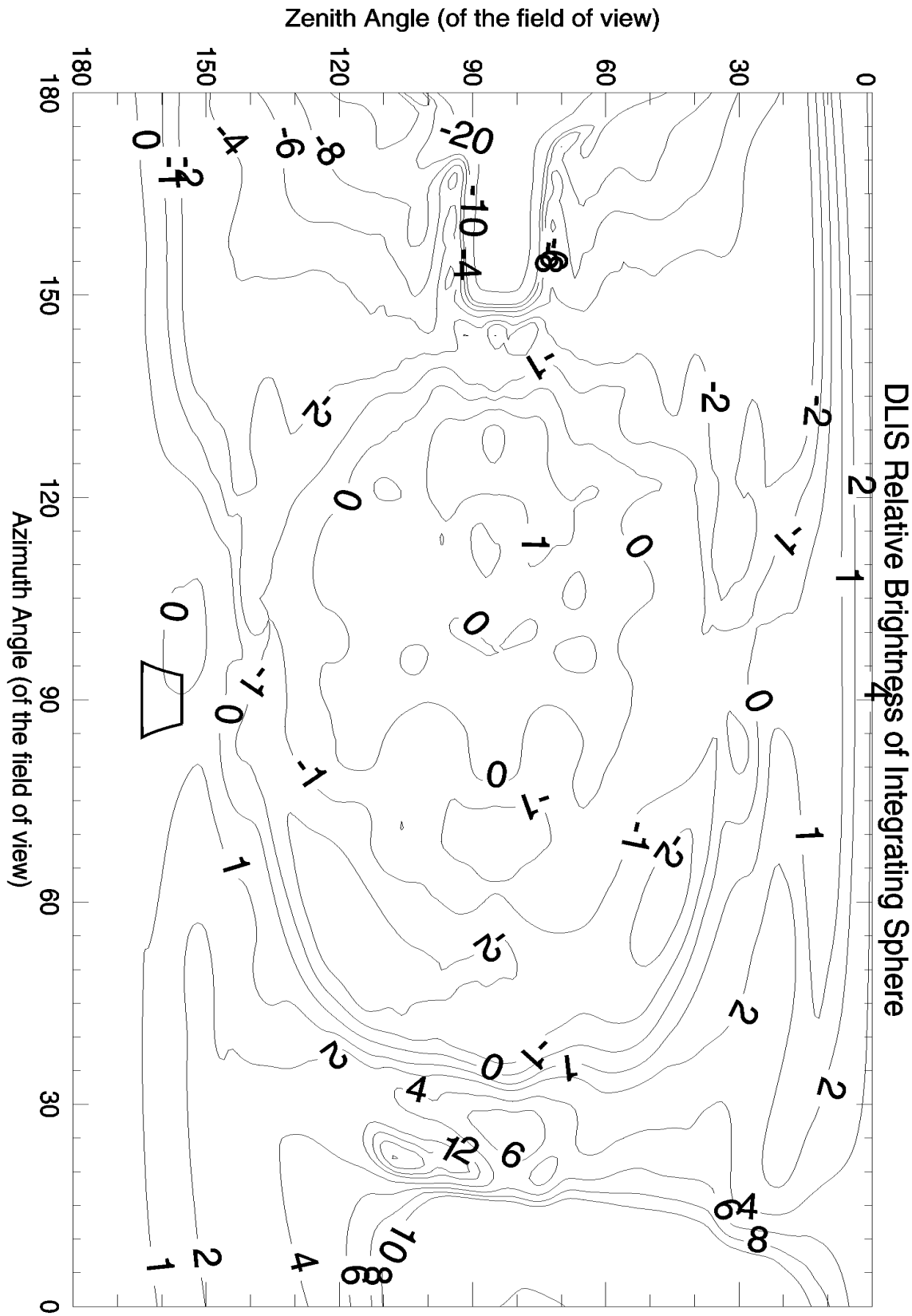
DLIS Relative Brightness of Integrating Sphere
Zenith Angle (of the field of view)
Azimuth Angle (of the field of view)
0
30
60
90
120
150
180

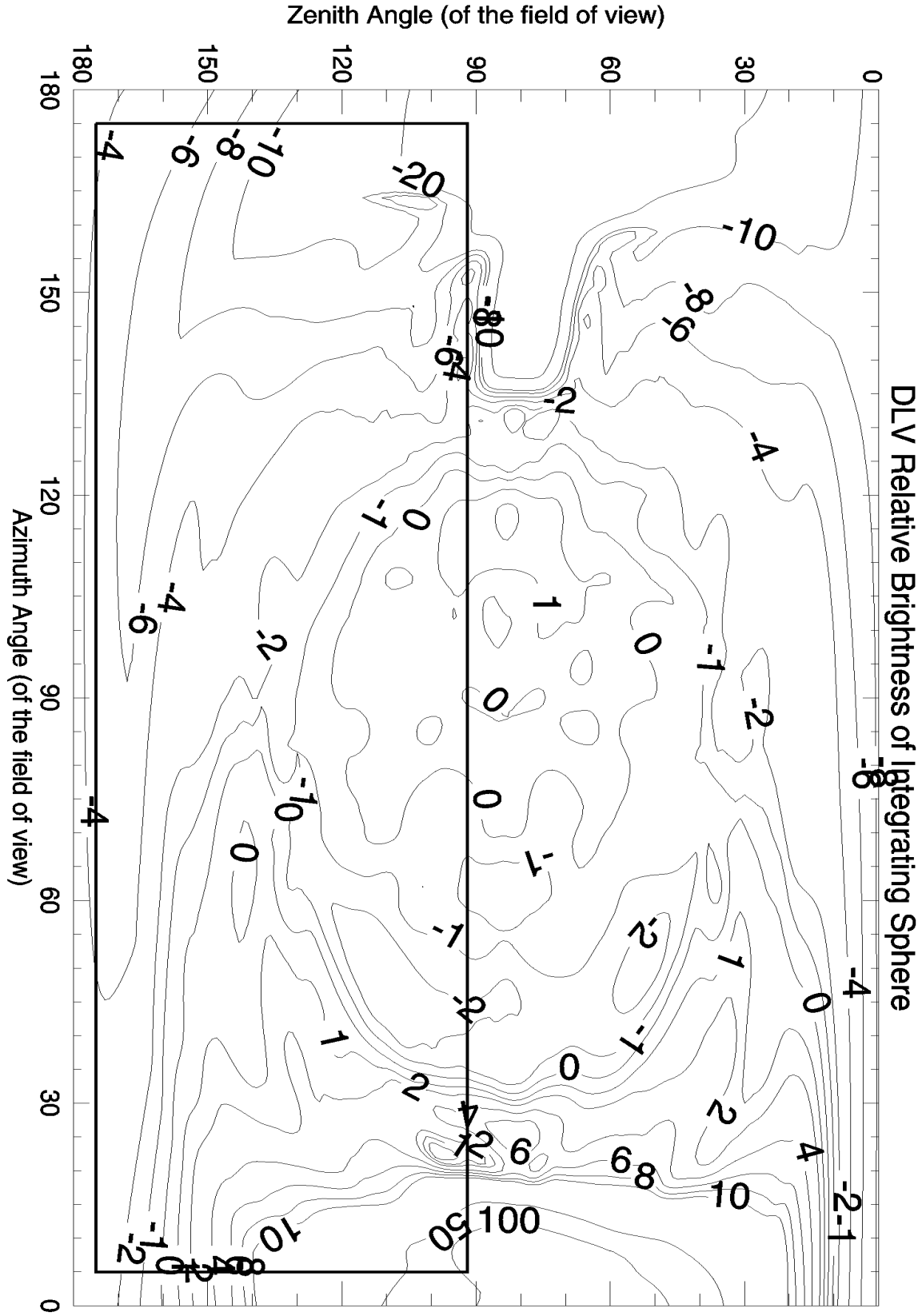
DLV Relative Brightness of Integrating Sphere
Zenith Angle (of the field of view)
Azimuth Angle (of the field of view)
0
30
60
90
120
150
180

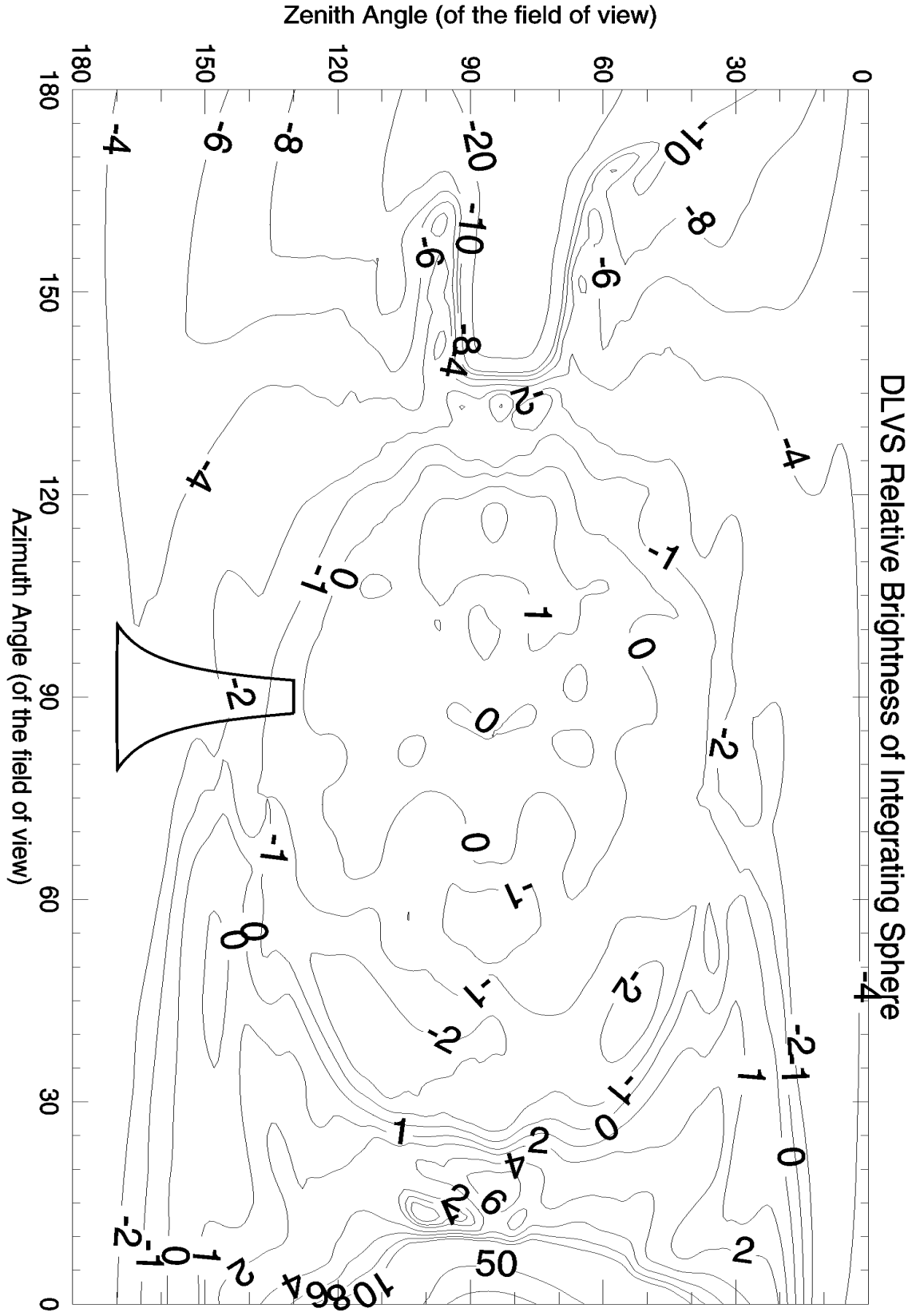
DLVS Relative Brightness of Integrating Sphere
Zenith Angle (of the field of view)
Azimuth Angle (of the field of view)
0
30
60
90
120
150
180

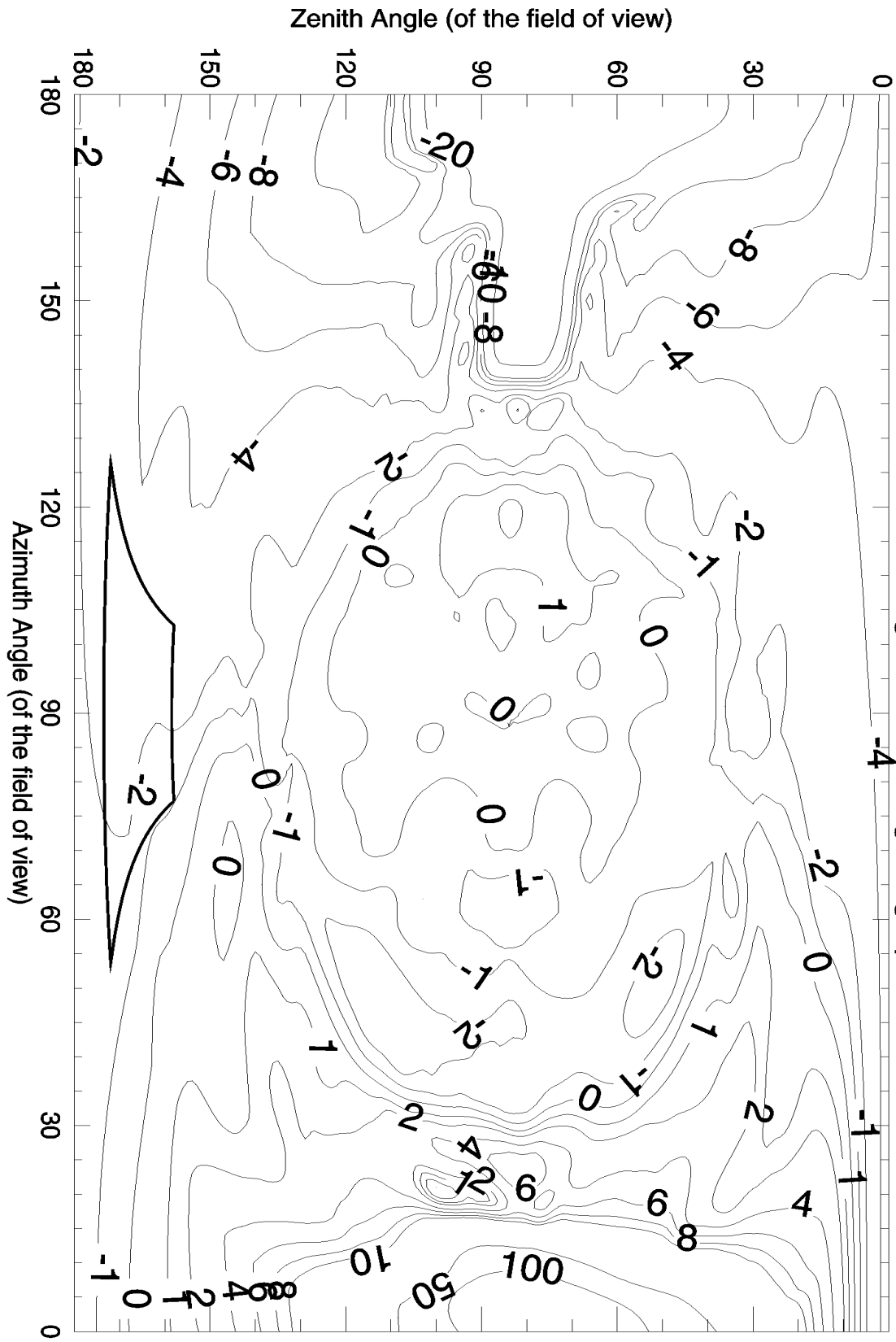
HRI Relative Brightness of Integrating Sphere
Zenith Angle (of the field of view)
Azimuth Angle (of the field of view)
0
30
60
90
120
150
180

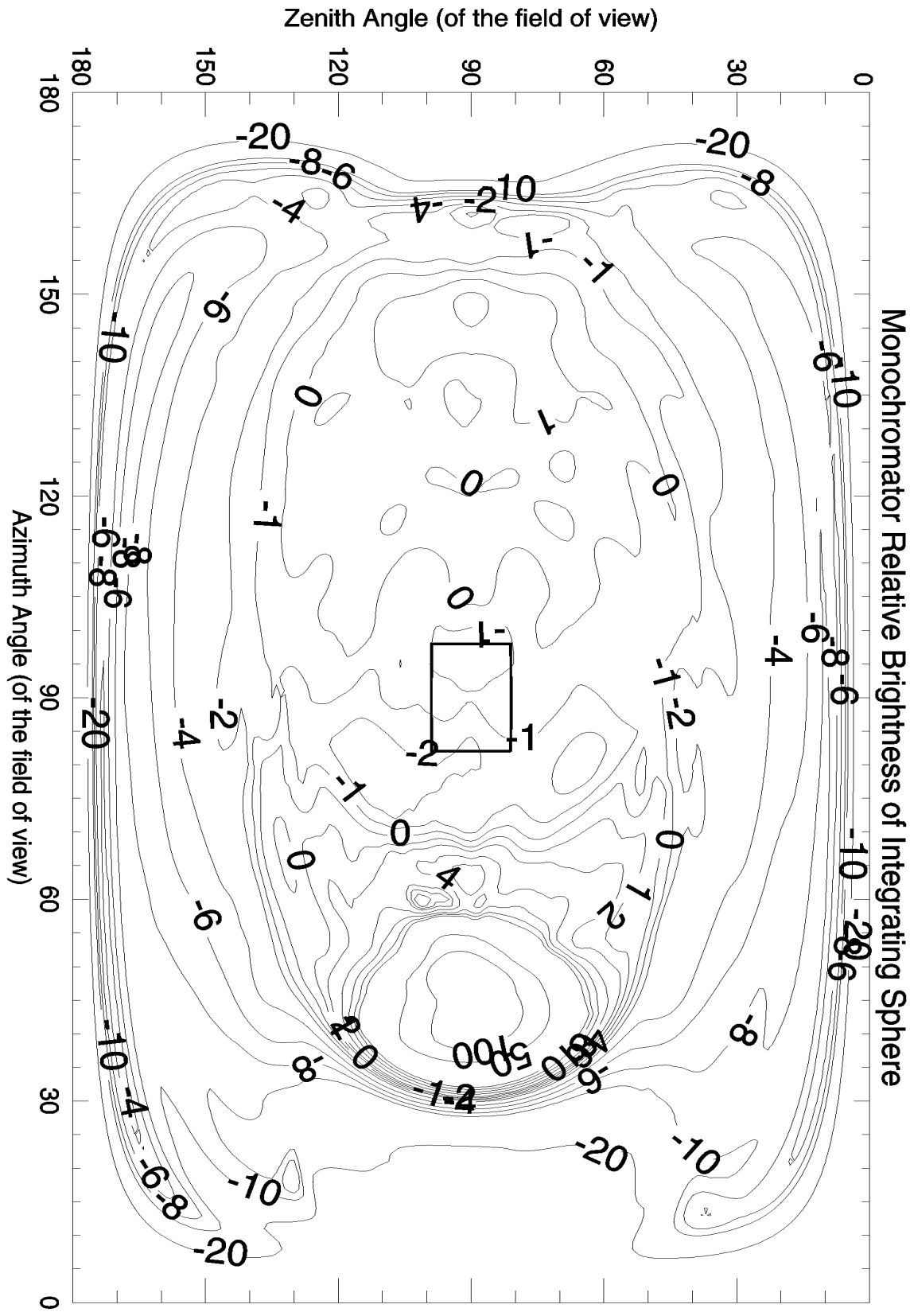
Monochromator Relative Brightness of Integrating Sphere
Zenith Angle (of the field of view)
Azimuth Angle (of the field of view)
0
30
60
90
120
150
180

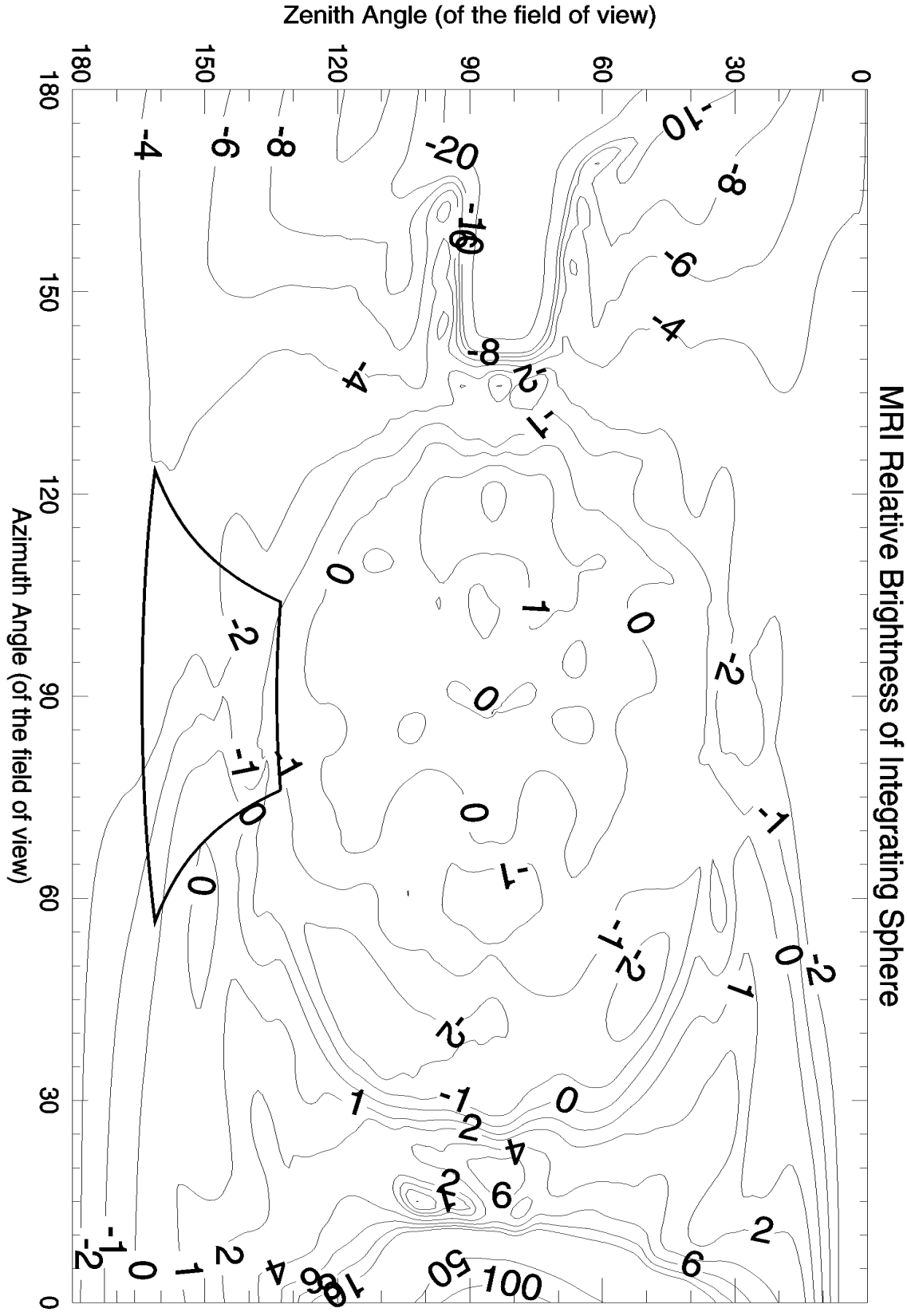
MRI Relative Brightness of Integrating Sphere
Zenith Angle (of the field of view)
Azimuth Angle (of the field of view)
0
30
60
90
120
150
180

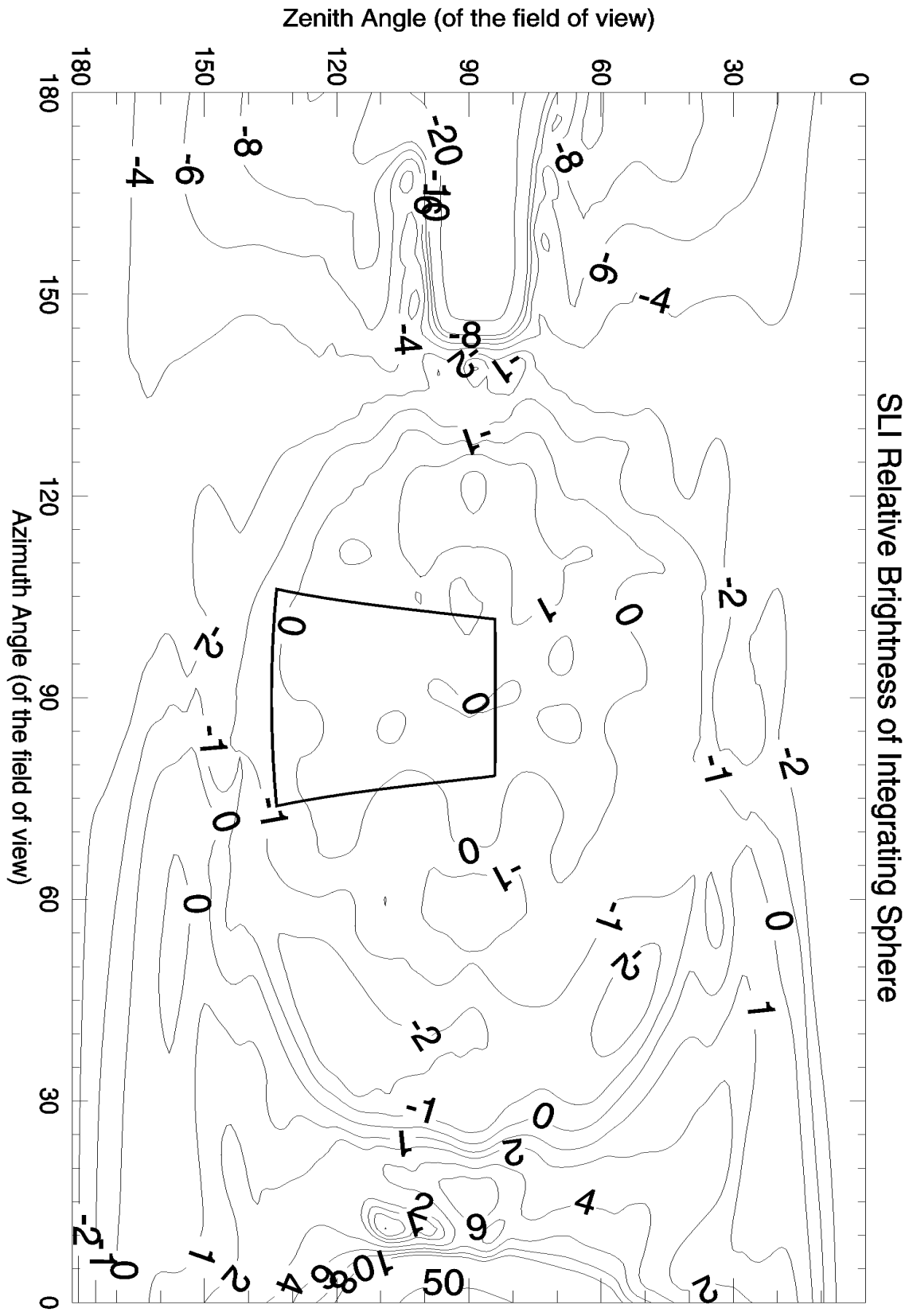
SLI Relative Brightness of Integrating Sphere
Zenith Angle (of the field of view)
Azimuth Angle (of the field of view)
0
30
60
90
120
150
180

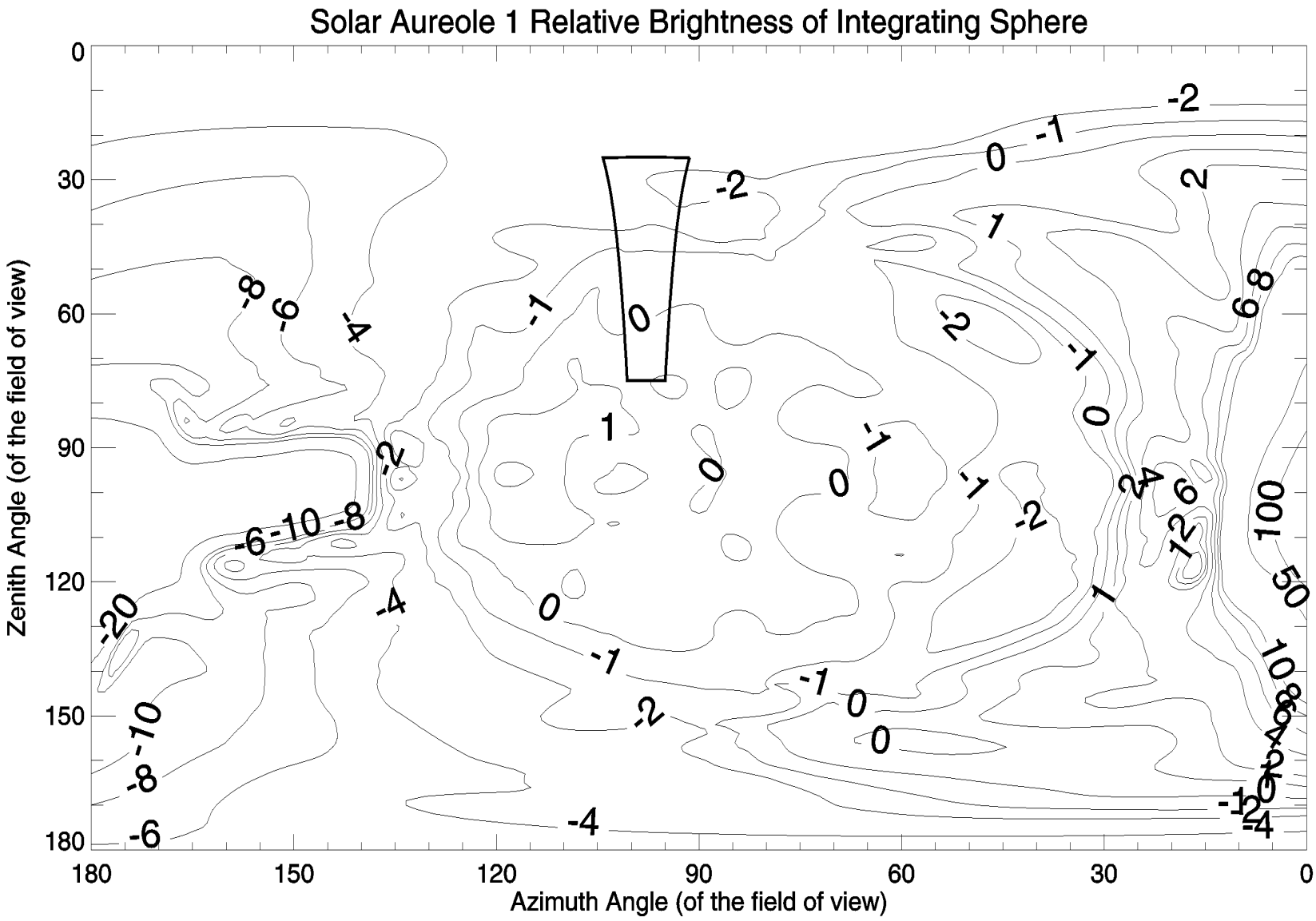
Solar Aureole 1 Relative Brightness of Integrating Sphere
Zenith Angle (of the field of view)
Azimuth Angle (of the field of view)
0
30
60
90
120
150
180
180
150
120
90
60
30
0

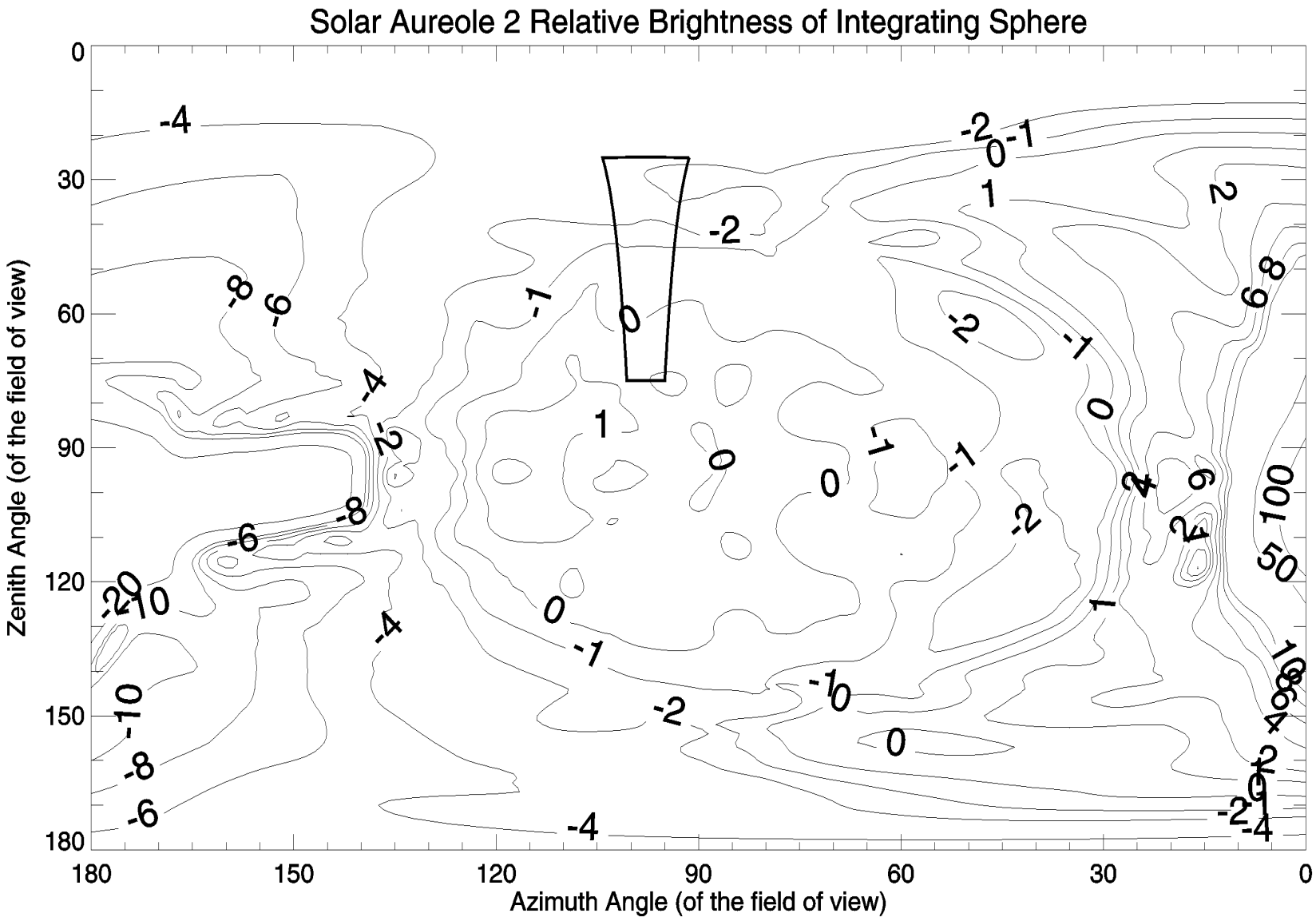
Solar Aureole 2 Relative Brightness of Integrating Sphere
Zenith Angle (of the field of view)
Azimuth Angle (of the field of view)
0
30
60
90
120
150
180
180
150
120
90
60
30
0

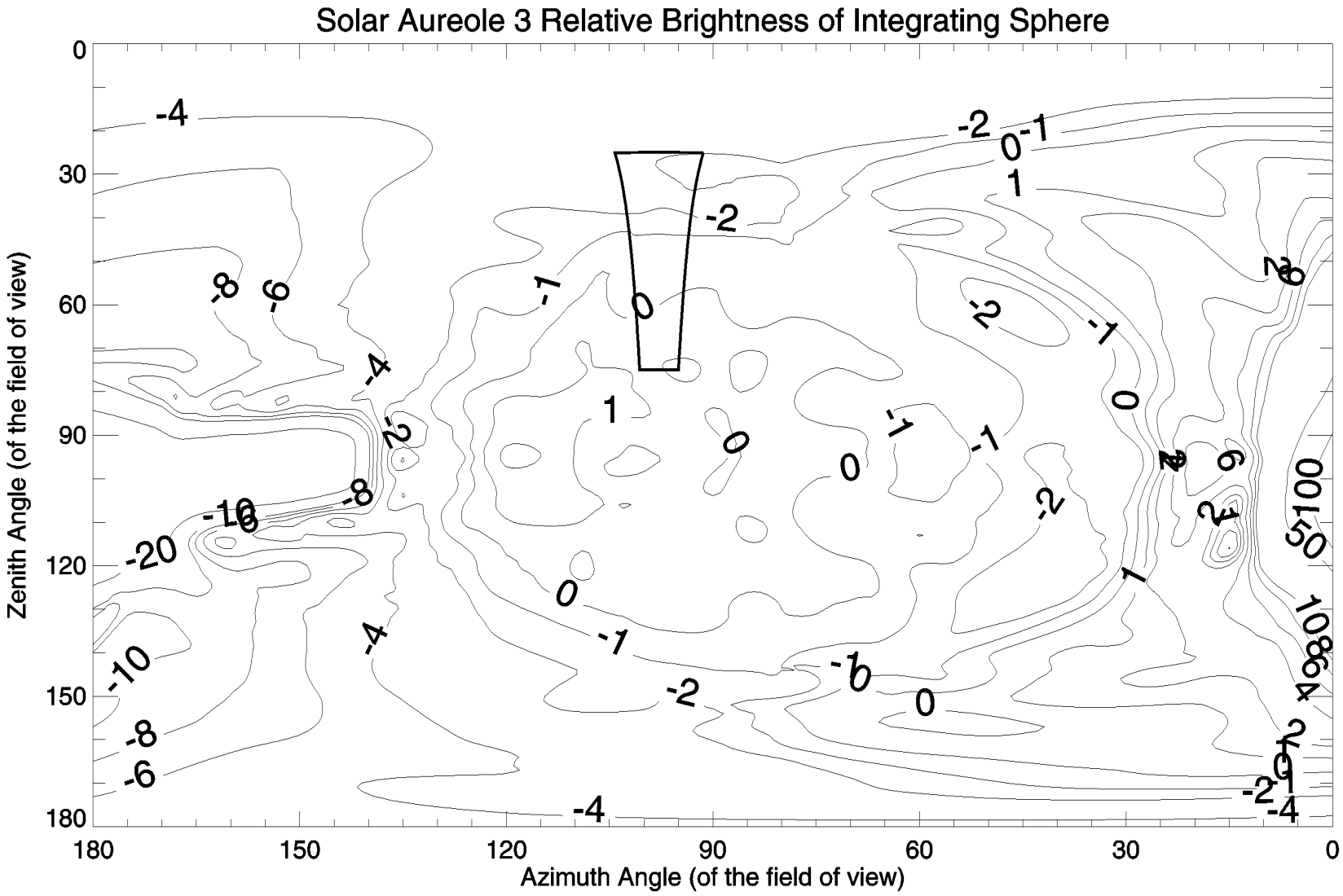
Solar Aureole 3 Relative Brightness of Integrating Sphere
Zenith Angle (of the field of view)
Azimuth Angle (of the field of view)
0
30
60
90
120
150
180
180
150
120
90
60
30
0

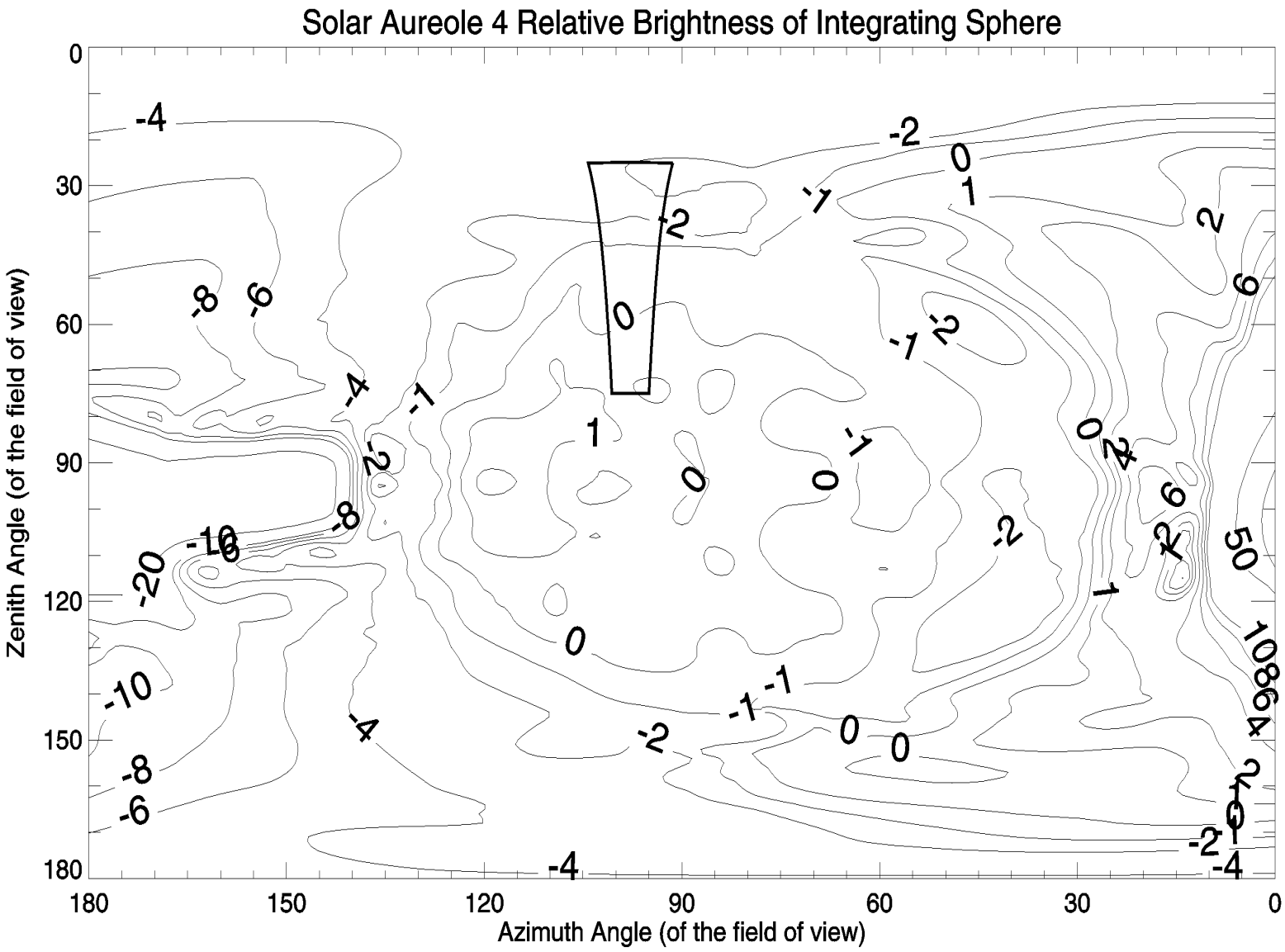
Solar Aureole 4 Relative Brightness of Integrating Sphere
Zenith Angle (of the field of view)
Azimuth Angle (of the field of view)
0
30
60
90
120
150
180
180
150
120
90
60
30
0

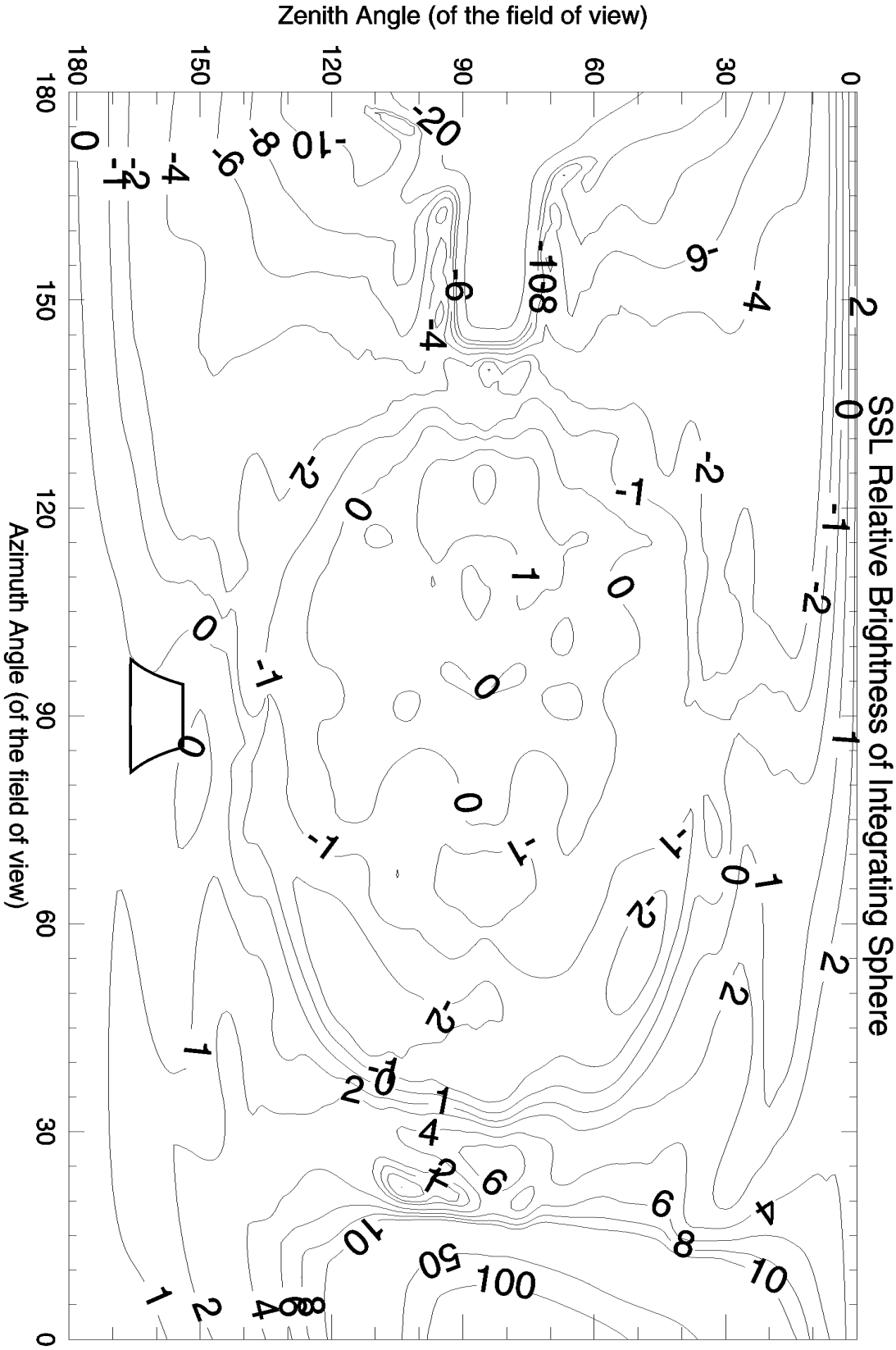
SSL Relative Brightness of Integrating Sphere
Zenith Angle (of the field of view)
Azimuth Angle (of the field of view)
0
30
60
90
120
150
180

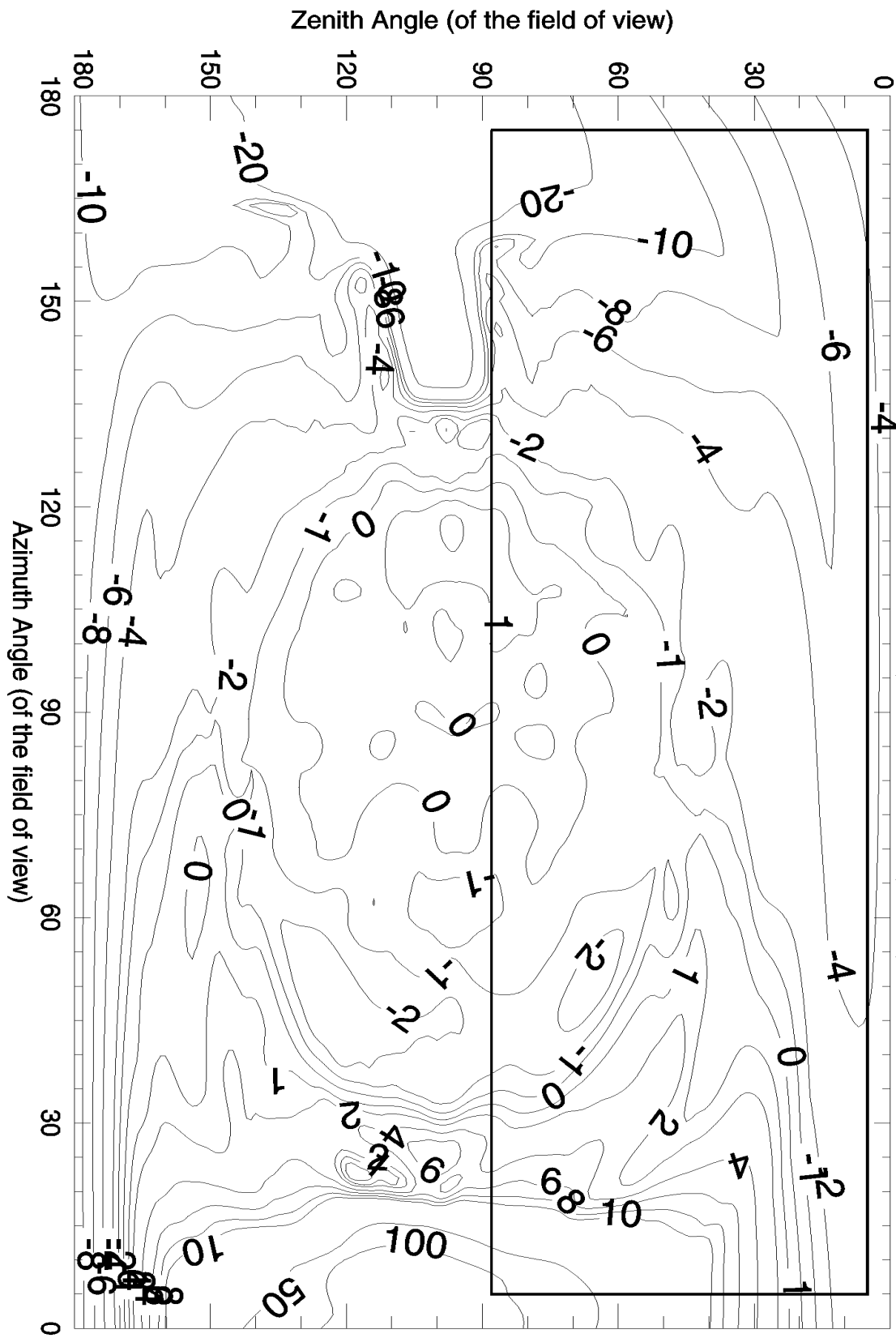
ULVS/ULV Relative Brightness of Integrating Sphere
Zenith Angle (of the field of view)
Azimuth Angle (of the field of view)
0
30
60
90
120
150
180

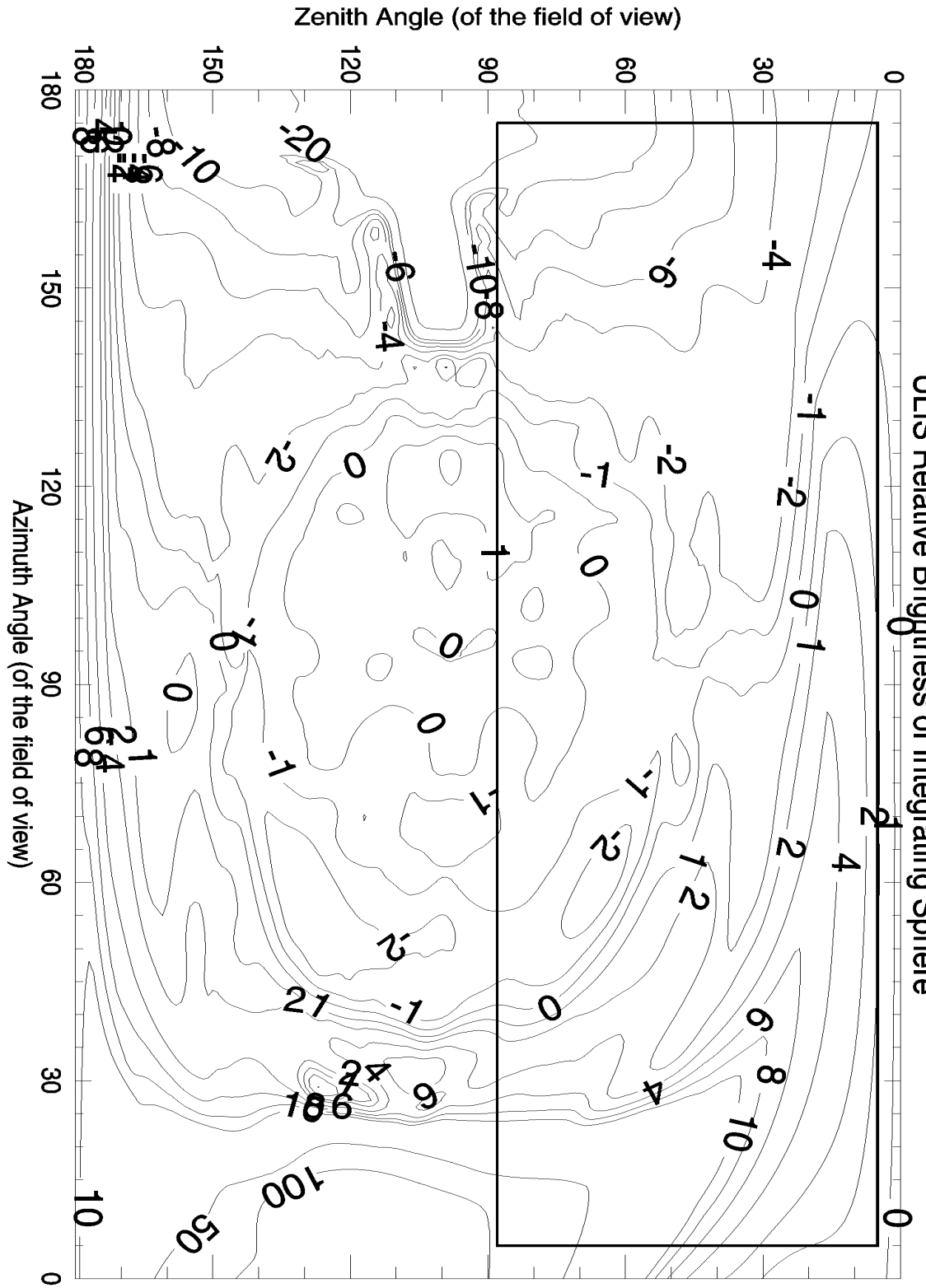
ULIS Relative Brightness of Integrating Sphere
Zenith Angle (of the field of view)
Azimuth Angle (of the field of view)
0
30
60
90
120
150
180

Appendix C: Relative Brightness Tables

The brightness tables are contained in the following files:

DLIS.ASC
DLV.ASC
DLVS.ASC
HRI.ASC
MONO.ASC
MIR.ASC
SA1.ASC
SA2.ASC
SA3.ASC
SA4.ASC
SLI.ASC
SS.ASC
SSL.ASC
ULIS.ASC
ULVS_ULV.ASC

And also in totality in:
Integrating_Sphere_Relative_Brightness.xls